Title
Investigation of Notch3-dependent mechanisms in KRAS-mutant lung adenocarcinoma

Author
Hwang, Elizabeth Eujin

Publication Date
2022

Investigation of Notch3-dependent mechanisms in KRAS-mutant lung adenocarcinoma

by
Elizabeth Hwang

DISSERTATION
Submitted in partial satisfaction of the requirements for degree of
DOCTOR OF PHILOSOPHY

in

Biomedical Sciences

in the

GRADUATE DIVISION
of the
UNIVERSITY OF CALIFORNIA, SAN FRANCISCO

Approved:

DocuSigned by:
KEVIN SHANNON
6F9DD324E1BF466...
KEVIN SHANNON
Chair

DocuSigned by:
Rushika Perera
Rushika Perera

DocuSigned by:
Melissa Reeves
Melissa Reeves

DocuSigned by:
Alejandro Sweet-Cordero
C48D20E9BBE844B...
Alejandro Sweet-Cordero

Committee Members

ACKNOWLEDGEMENTS

When I began this journey 7 years ago as a new first-year, little did I know how long and arduous of a journey I was about to embark on. Yet throughout the highs and lows of this path, I have also forged meaningful and rewarding relationships with among the most brilliant and kind people I have ever encountered in both my personal and professional lives, a few of whom I have the privilege to acknowledge here:

My class of 2015 MSTP cohort, particularly Ugomma, Antonia, Sara, and Paul, who listened, commiserated, and cheered me on every step of the way. My ever-patient Williams College friends: Shirl, Uttara, CC, Sora - how far we have come since our deep late-night discussions in Schow, Jesup, and wherever there were comfy couches or free food. My lab members to whom I owe my deepest gratitude for the friendship and knowledge they have so generously shared over these difficult years, and particularly David, who will probably be the only person to read this page. May we enjoy many beers together in the future.

Of course, Alejandro, who accepted me into his lab without hesitation or doubt, and who has challenged my thinking again and again. And my incredible committee members, who were truly the best decision I ever made as a graduate student: Melissa, Rushika, and Kevin, I could not have finished this without your support. Finally, my family: Mom, Dad, Ariel, and Robert, who not only accepted my decision to enter a program with no clear end-date on the other side of the country, but also believed in me regardless of what lay ahead.

Let me illustrate by a case of my own. There is a mutant called "notch" characterized by a serration at the ends of the wings ... there is present a new and definite gene that does account for the change.

- The Theory of the Gene, 1917, Professor T.H. Morgan

INVESTIGATION OF NOTCH3-DEPENDENT MECHANISMS IN LUNG ADENOCARCINOMA

ELIZABETH HWANG

ABSTRACT

Lung adenocarcinoma (LUAD) is a highly heterogeneous disease with recurrent driver mutations. Given the recent increase in targeted therapies, many of these are now considered "actionable" mutations, yet clinical trials continue to show limited improvements in patient overall survival. Thus, there is an urgent need to identify the key pathways and regulators underlying tumor progression and drug resistance. Here, we investigate the role of Notch3, a known regulator of epithelial lung development previously implicated in tumor-propagation capacity, in the LUAD context. We demonstrate that, while Notch activity is not required for cell survival, Kras-mutant LUAD cells undergo epithelial-to-mesenchymal transitional (EMT) state changes in response to both direct and indirect mechanisms engaged by transcriptionally active Notch3. We use transcriptomic and epigenetic analyses to define a set of Notch3 target genes and utilize genome-wide screening approaches to show that a subset of these regulate Notch3-induced therapeutic resistance to covalent Kras(G12C) inhibition. Given recent clinical data from patients and preclinical in vitro models supporting a role for EMT in Kras(G12C) resistance, our datasets provide unique epigenetic and transcriptional resources to discover potential therapeutic targets for overcoming resistance and subsequent tumor progression.

TABLE OF CONTENTS

LIST OF FIGURES

LIST OF TABLES

CHAPTER 1

BACKGROUND

Notch: A Master Regulator of Development

Cell-cell communication is an essential component of any successful attempt at organismal evolution, development, and survival. In particular, multicellular eukaryotes universally rely upon Notch signaling to act as a cornerstone of embryogenesis coordination as well as adult stem cell maintenance.

Historically, the classic "notched wing" *Drosophila* mutants, for which the gene family is named, were first identified as heritable traits by John S. Dexter in 1914[1]. Shortly afterwards, Thomas Hunt Morgan attributed this phenotype to a dominant, sex-linked mutation that could be carried in both a dominant and recessive fashion in females, but regardless was always lethal in males[2]. The complexity of hereditary patterns and phenotypes with Notch mutants led to difficulties in ascribing a single developmental function to the Notch gene. Donald Poulson in the 1930s used *Drosophila* mutants with truncated chromosomes missing the "Notch" locus to discover its role embryogenesis, as his mutants failed to develop the mesoderm and endoderm during gastrulation[3].

Finally in 1983, Spyros Artavanis-Tsakonas cloned the first sequence of the *Notch* gene[4], and noted the 36 cysteine-rich repeats with high homology to the EGF sequence, comparable to those discovered in similar proteins with extracellular domains. Hence, Wharton et al. proposed Notch to be a transmembrane receptor, and from there other labs followed with the sequencing of Notch ligands, which had similar EGF repeats and structure.

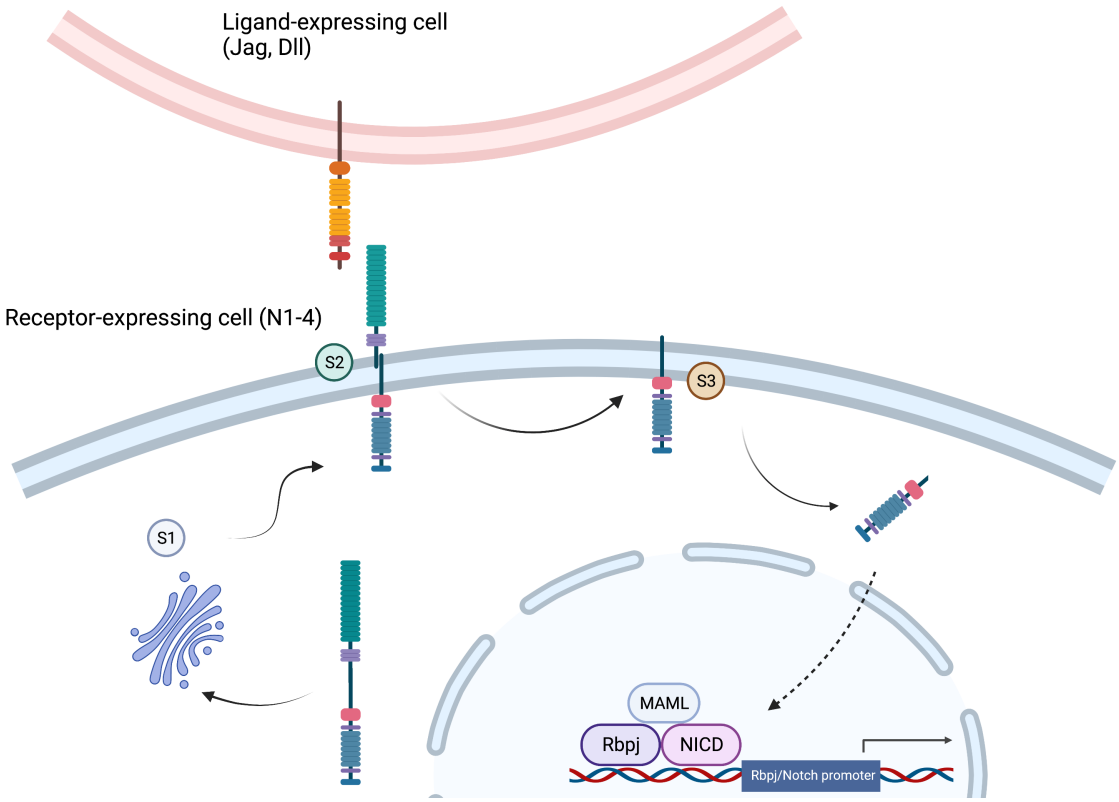

Figure 1.1 The Notch Signaling Pathway The full-length Notch receptor is modified in the endoplasmic reticulum (not show) and undergoes its first S1 proteolytic cleavage at the Golgi apparatus, producing a Notch-extracellular domain (NECD) and intracellular domain (NICD) heterodimer. The EGF-repeat like region in the NECD facilitate ligand binding (via the ligand's ECD), resulting in a conformational change that exposes the receptor's negative regulatory region (NRR) which then undergoes sequential S2 cleavage by ADAM (a disintegrin and metalloprotease) family members and followed by gamma-secretase mediated S3 cleavage. The released NICD contains a nuclear localization signal (NLS) and, possibly via endocytosis, localizes to the nucleus where it complexes with the common Notch transcription factor, Rbpj/CSL, and the MAML transcriptional activator to initiate transcription. The Notch Transcriptional Complex (NTC) refers to the ternary Rbpj-NICD-MAML complex. Figure made in Biorender, adapted from Salazar and Yamamoto et al. (2018, *Molecular Mechanisms of Notch Signaling*)

At its core, the Notch pathway appears deceptively simple: a single membrane-associated receptor engages a single heterotypic (cell to neighbor cell) ligand via their respective EGF-like repeat domains, resulting in the receptor undergoing a conformational change, sequential and cleavages by ADAM metalloproteinases (S2) and gamma secretase (S3), and the release of an active intracellular fragment which will complex with a common transcription factor (Rbpj) and activator (MAML) to initiate a Notch transcriptional program[5,6] (**Figure 1.1**). This is considered

a one-to-one signaling pathway. By contrast, most other growth-factor pathways which utilize secondary messengers to specify the degree and duration of signal output. Furthermore, the pathway appears quite vulnerable, as loss of Rbpj or a dominant negative mutation in a single component (e.g. the MAML transcriptional activator) can readily shut down all transcriptional activity. Yet there have been increasing hints at a far more complex regulatory network: as evidence of intracellular ligand signaling[7–10], homotypic (cell to self) receptor-ligand interactions[11], and non-canonical roles of Notch, including but not limited to transcriptional regulation[12], have surfaced over the last decade, it has become clear that the Notch signaling pathway has a greater capacity for adaptation and modulation than initially recognized.

Notch signaling in development primarily functions in two inter-related roles, lateral inhibition and boundary development[13]. Together, these function to direct tissue organization through Notch-mediated direction of cell fate. An elegant example of this is demonstrated in neurodevelopment, where *in vivo* single-cell time-lapse imaging of zebrafish forebrain development and clonal analysis of individual radial glial lineages revealed that Notch regulates the decision pathways leading to cell fate[14]. Asymmetric cell division in this system is established by the intrinsic polarity regulator partitioning defective protein 3 (Par3), which segregates Mindbomb, a ubiquitin ligase regulating internalization of the intracellular domain[15], to the apical daughter cell and thereby restricts Notch signaling to the basal daughter cell. The resultant differential Notch activity promotes self-renewal in the basal cell (high Notch) and differentiation of the apical daughter (low Notch), illustrating how self-renewal and differentiation are segregated in asymmetrically dividing neural stem/progenitor cells of the same lineage, ultimately resulting in the formation of cortical layer boundaries.

Notch1, the first of four mammalian Notch paralogs identified, was discovered by Leif Ellisen through a recurrently occurring translocation in T-cell acute lymphoblastic leukemia (T-ALL) with high homology to the *Drosophila* Notch gene[16]. Since then, three more Notch paralogs (Notch2, Notch3 and Notch4) have been described in mammals and are believed to have arisen through gene duplication and the evolution of functional diversification likely through acquisition of structural differences[17]. Notably, only Notch1 and Notch2 are believed to be essential for mammalian development as *in vivo* knockout models of these are embryonic lethal, while those of Notch3 and Notch4 are not[18,19]. This is most likely attributable to the restricted expression of the latter receptors, which primarily occur in vasculature smooth muscle, neuroepithelium, thymocytes and T-lymphocytic lineages[18] (Notch3) and in vascular endothelial cells[20] (Notch4). This is not to argue that they are less developmentally relevant, as pathogenic mutations of the Notch3 extracellular domain are associated with CADASIL, an inheritable small-vessel disease causing stroke and dementia, and the causality of these pathogenic mutations have been demonstrated through *in vivo* mouse modeling[21].

Structurally, Notch3 is unique in that its intracellular domain (Notch-ICD, or NICD) was thought to have a "weaker" transactivation domain (TAD), as determined by upregulation of the canonical Notch target Hes1, relative to the Notch1/2 ICDs (the Notch4-ICD lacks any TAD entirely)[22]. However, several pieces of evidence suggest that NICD3 may have evolved to act in a transcriptionally distinct manner from NICD1/2: First, NICD3 has a unique ankyrin domain, suggesting its protein-protein interaction preferences are unique from NICD1/2[22]. Second, it has been shown that NICD1 and NICD3 have different DNA binding preferences at Rbpj/CSL sites. Such sites often occur as paired consensus repeats, thought to facilitate cooperative binding of dimeric Notch transcriptional complexes (NTCs, Rbpj/Notch-ICD/MAML), or in their absence,

dimeric Rbpj, resulting in gene repression. *In vitro*, NICD1 appears to more strongly activate paired CSL sites[23] and NICD3 prefers single CSL sites, though the latter appears to require additional *cis*-elements indicating NICD3 may require non-canonical binding partners[24]. A recent study of dimerization-deficient mutants of the four Notch receptors found that the requirement for dimerization is promoter-dependent[25], carrying implications for their ability to regulate specific targets: for example, Hes5 and Hey1 regulation are dimer-independent, while Hes1 is strongly dimer-dependent[26]. Together, these observations support a role for unique Notch1- and Notch3-transcriptional programs.

Lung Cancer Epidemiology

Lung cancer is the leading cause of cancer-related deaths both in the United States[27] and worldwide[28]. As the second-most frequently diagnosed cancer among adults with over 230,000 new diagnosed cases projected for 2022[27], lung cancer continues to carry among the highest morbidity as well as mortality rates of all malignancies, despite the recent decreases in incidence due to a decline in smoking in the general U.S. population. Lung cancers can be broadly classified into either small cell (SCLC) or non-small cell lung cancer (NSCLC), respectively representing about 15% and 85% of all cases. SCLC is a rapidly growing, neuroendocrine tumor that typically presents with metastasis and is found nearly exclusively in smokers[29], while NSCLC encompasses a number of subtypes which can occur in both smokers and non-smokers. NSCLC can be further subtyped into two predominant histologies: adenocarcinoma (LUAD, 50%), which is identified by glandular histology and staining for distal alveolar biomarkers (SPC, KRT7, TTF1) and squamous cell carcinoma (LUSC, 40%), is distinguished by morphology resembling the pseudostratified columnar epithelium which lines the proximal airways where it arises and may feature keratinization. Pathologic diagnosis of LUSC is

confirmed through immunohistochemical staining of nuclear p63/p40, with or without SOX2 and KRT5/6, as definitive markers for squamous differentiation[30,31].

In addition to differences in histology, LUAD and LUSC also differ in their identified driver mutations. LUAD frequently contain mutations in EGFR (10%) or KRAS (25%-30%), and less frequently in HER2, BRAF, and non-Kras RAS genes, while LUSC most often harbor amplifications in FGFR1 (22%), PI3KCA (33%) or MET (5%)[30]. A smaller subset of LUAD are driven by ALK or ROS1 rearrangements (~6%)[32]. Many genomic alterations in LUAD are now directly actionable through targeted therapies, such as EGFR, BRAF, ALK/ROS1 rearrangements, and more recently, KRAS[33]. However, despite the development of multiple FDA-approved targeted agents, few clinical trials have shown increases in overall survival and nearly all tumors treated with monotherapy regimes eventually progress[34]. Consequently, there has been significant interest in understanding the determinants of therapeutic sensitivity/resistance and tumor progression, particularly in the context of dominant oncogenic drivers such as mutant EGFR and KRAS.

KRAS-mutant lung adenocarcinoma: a newly-targetable disease

Among the LUAD driver mutations, KRAS mutations have long been of interest for several reasons: first, the historical significance of the RAS family as oncogenes, second, the high prevalence of KRAS mutations in LUAD, and third, the availability of genetically engineered mouse models (GEMMs) to examine the underlying developmental origins and progression of this disease.

RAS genes were first isolated as the transforming agents carried by tumorigenic retroviruses derived from model animals (*ra*t *s*arcomas)[35]. Following the discovery of v-src's avian origin in 1976 by Varmus and Bishop[36,37], a series of experiments led by Scolnick at the

NCI resulted in the identification of endogenous HRAS[38] and KRAS[39] genes and their function as membrane-bound GTPases[40]. Since then, the RAS family members have been firmly established as the most commonly mutated oncogenes in human cancers[35] and demonstrated to exert a wide range of effects upon cellular processes.

Three genes encode for the four 21 kDa proteins which comprise the RAS family: HRAS, NRAS, KRAS4A and KRAS4B (isoforms encoded by alternative exon 4 usage). These membrane-bound small GTPases physically interact with downstream signaling partners via an exposed effector loop, whose binding affinity is regulated by the binding of GTP (high affinity) or GDP (low affinity). Intrinsically, the ratio of the active GTP-bound to inactive GDP-bound state is determined by the rates of GTP hydrolysis and GDP exchange. Extrinsically, the cycling between states is a key regulatory point for the RAS proteins and is tightly regulated by the availability of GDP-exchange factors (GEFs) and GTPase-activating proteins (GAPs). GEFs, which promote a GTP-bound state, activate RAS signaling while GAPs are repressive, and both are also found mutated in RAS-driven cancers[35]. In RAS-mutant cells, extracellular stimulation through receptor tyrosine kinases, such as EGFR, results in an outsized signaling response which ultimately promotes growth, proliferation and survival. The exact downstream pathways are engaged in a mutation- and cell context-dependent manner, but often include some combination of MEK/ERK, PI3K/AKT, and RALGDS, among others[41].

Despite sharing between 80-90% sequence identity, the RAS isoforms demonstrate exquisite specificity in histological expression both in normal development and in tumors[42]. While single-mutant deficiencies are not necessarily embryonically lethal (with the exception of KRAS4B), the RAS proteins are thought to be largely non-redundant and show distinct preferences for cellular localization, which likely reinforces their differential activation of

downstream signaling pathways. One of the strongest arguments for the lack of redundancy between the family members is the high degree of selectivity for isoform and mutational profiles between cancer subtypes: for example, RAS mutations in NSCLC are almost exclusively found in KRAS, while the same is true of NRAS mutations in melanoma. Because of their high structural similarity, nearly all mutations are found in codons 12, 13 and 61, increase the ratio of GTP-to-GDP-bound Ras and thereby increase signal output. Interestingly, the preferred amino acid change appears to also vary by isoform and cancer subtype. In LUAD, nearly half (46%) of KRAS mutations occur as G12C mutations, while the rest are largely seen in G12V (23%), G12D (17%), and G12A (10%)[43]. These function primarily by render mutant KRAS insensitive to GAPs[44], notably p120 RASGAP and neurofibromin, as well as decreasing the rate of intrinsic nucleotide exchange[45].

Over the past decade, the development of novel Kras(G12C) inhibitors has rapidly altered the face of therapeutic avenues for Kras-mutant NSCLC patients. In 2013, the Shokat lab at UCSF published the groundbreaking discovery of small molecule inhibitors covalently targeting the switch II pocket region of G12C mutant Kras via its cysteine residue, locking the Kras(G12C) oncogene into its GDP-inactive state[33]. Since then, the pharmaceutical industry and academic labs have been engaged in an arms race to develop not only compounds with improved pharmacologic properties, but also non-covalent inhibitors capable of targeting non-G12C mutant Kras[46], potentially widening the eligible patient population to predominantly Kras G12D-mutant cancers such as colorectal and pancreatic adenocarcinomas.

Yet early clinical trial from G12C inhibitors already suggests that while Kras-targeting monotherapy is capable of preventing disease progression, even in highly pre-treated and advanced tumors, most tumor types outside of NSCLC fail to respond[47] and nearly all treated

tumors will eventually acquire resistance. Oftentimes, resistance mutations appear to occur in Kras itself, whether through manifestation of a non-G12C missense mutation in an hetero-allelic fashion or through *de novo* mutations at other sites such as Q61. A detailed study of patients with acquired resistance to adagrasib, an orally available Kras G12C inhibitor developed by Mirati, highlighted the importance of RTK-RAS-MAPK signaling in these resistant tumors, a number of which were found to harbor activating mutations or gene fusions in Ras/Raf family members, or MET amplification[48], while 11/38 enrolled patients had no identifiable mutations by targeted next-generation sequencing. As evidence of non-genetic mechanisms of resistance, two NSCLC cases demonstrated histologic transformation from adenocarcinoma to squamous cell carcinoma, though in many of the cases, histology was not assessed due to a lack of available post-relapse tissue[48]. Overall, these findings paint a clinical picture of Kras-mutant cancers as a heterogenous group of often highly aggressive disease course which will require combinatorial approaches for optimal chances at tumor response and suppression of intrinsic or acquired resistance.

Current Perspectives

Despite the promise of improved treatment strategies for Kras-mutant NSCLC, these novel inhibitors underscore a key limitation of targeted cancer therapies — uncertainty regarding which patients will respond to treatment, and for how long. While preclinical trial data can provide some answers to potential combination therapies, the development of new rationale therapeutic strategies requires a molecular understanding of tumor resistance and ideally, a mechanistic model to predict disease response.

In this report, we study the contribution of the Notch developmental pathway to the cell state and survival of lung adenocarcinoma. We have focused on utilizing Kras-mutant cell line models, both from the primary LUAD GEMM as well as patient-derived. This work is divided

into two parts: We first assess the requirement for active Notch signaling in our cell line models by using small molecule inhibitors of Notch intracellular domain (S3) cleavage to show a lack of dependence on transcriptional signaling *in vitro*. Second, we engineer an inducible model of the tagged-Notch3 intracellular domain (NICD3), expressed in human Kras-mutant LUAD cell lines, and define a Notch3-driven transcriptional and epigenomic program. We proceed to demonstrate Notch3 transcriptional activation as a potential mechanism of resistance to Kras(G12C) inhibition and that this effect is likely mediated through an epithelial-to-mesenchymal (EMT) developmental program. Together, our results highlight a broader role for Notch3 signaling in NSCLC tumor progression and targeted therapy resistance.

REFERENCES

1. Dexter, J. S. The Analysis of a Case of Continuous Variation in Drosophila by a Study of Its Linkage Relations. *The American Naturalist* **48**, 712–758 (1914).

2. Morgan, P. T. H. The Theory of the Gene. *The American Naturalist* **51**, 33 (1917).

3. Poulson, D. F. Chromosomal Deficiencies and the Embryonic Development of Drosophila Melanogaster. *Proc. Natl. Acad. Sci. U.S.A.* **23**, 133–137 (1937).

4. Wharton, K. A., Johansen, K. M., Xu, T. & Artavanis-Tsakonas, S. Nucleotide sequence from the neurogenic locus Notch implies a gene product that shares homology with proteins containing EGF-like repeats. *Cell* **43**, 567–581 (1985).

5. *Molecular Mechanisms of Notch Signaling*. vol. 1066 (Springer International Publishing, 2018).

6. Radtke, F., Schweisguth, F. & Pear, W. The Notch 'gospel'. *EMBO Rep* **6**, 1120–1125 (2005).

7. Chakrabarti, R. *et al*. Notch ligand Dll1 mediates cross-talk between mammary stem cells and the macrophageal niche. *Science* **360**, eaan4153-14 (2018).

8. Choi, K. *et al*. Distinct biological roles for the notch ligands Jagged-1 and Jagged-2. *J Biol Chem* **284**, 17766–17774 (2009).

9. LaVoie, M. J. & Selkoe, D. J. The Notch Ligands, Jagged and Delta, Are Sequentially Processed by α-Secretase and Presenilin/γ-Secretase and Release Signaling Fragments. *J. Biol. Chem.* **278**, 34427–34437 (2003).

10. Yamamoto, S., Charng, W.-L. & Bellen, H. J. *Chapter Five - Endocytosis and Intracellular Trafficking of Notch and Its Ligands. Current Topics in Developmental Biology - Volume 92* vol. 92 200 (Elsevier Inc., 2010).

11. LeBon, L., Lee, T. V., Sprinzak, D., Jafar-Nejad, H. & Elowitz, M. B. Fringe proteins modulate Notch-ligand cis and trans interactions to specify signaling states. *Elife* **3**, 25477–24 (2014).

12. Andersen, P., Uosaki, H., Shenje, L. T. & Kwon, C. Non-canonical Notch signaling: emerging role and mechanism. *Trends in Cell Biology* **22**, 257–265 (2012).

13. Artavanis-Tsakonas, S., Rand, M. D. & Lake, R. J. Notch signaling: cell fate control and signal integration in development. *Science* **284**, 770–776 (1999).

14. Dong, Z., Yang, N., Yeo, S.-Y., Chitnis, A. & Guo, S. Intralineage directional Notch signaling regulates self-renewal and differentiation of asymmetrically dividing radial glia. *Neuron* **74**, 65–78 (2012).

15. Itoh, M. *et al*. Mind bomb is a ubiquitin ligase that is essential for efficient activation of Notch signaling by Delta. *Dev Cell* **4**, 67–82 (2003).

16. Ellisen, L. W. *et al*. TAN-1, the human homolog of the Drosophila Notch gene, is broken by chromosomal translocations in T lymphoblastic neoplasms. *Cell* **66**, 649–661 (1991).

17. Gazave, E. *et al*. Origin and evolution of the Notch signalling pathway: an overview from eukaryotic genomes. *BMC Evol Biol* **9**, 249 (2009).

18. Krebs, L. T. *et al*. Characterization of Notch3-deficient mice: normal embryonic development and absence of genetic interactions with a Notch1 mutation. *Genesis* **37**, 139–143 (2003).

19. McCright, B. *et al*. Defects in development of the kidney, heart and eye vasculature in mice homozygous for a hypomorphic Notch2 mutation. *Development* **128**, 491–502 (2001).

20. James, A. C. *et al*. Notch4 reveals a novel mechanism regulating Notch signal transduction. *BBA - Molecular Cell Research* **1843**, 1272–1284 (2014).

21. Lacombe, P., Oligo, C., Domenga, V., Tournier-Lasserve, E. & Joutel, A. Impaired cerebral vasoreactivity in a transgenic mouse model of cerebral autosomal dominant arteriopathy with subcortical infarcts and leukoencephalopathy arteriopathy. *Stroke* **36**, 1053–1058 (2005).

22. Beatus, P., Lundkvist, J., Oberg, C., Pedersen, K. & Lendahl, U. The origin of the ankyrin repeat region in Notch intracellular domains is critical for regulation of HES promoter activity. *Mech Dev* **104**, 3–20 (2001).

23. Nam, Y., Sliz, P., Pear, W. S., Aster, J. C. & Blacklow, S. C. Cooperative assembly of higher-order Notch complexes functions as a switch to induce transcription. *Proceedings of the National Academy of Sciences* **104**, 2103–2108 (2007).

24. Ong, C.-T. *et al*. Target selectivity of vertebrate notch proteins. Collaboration between discrete domains and CSL-binding site architecture determines activation probability. *J. Biol. Chem.* **281**, 5106–5119 (2006).

25. Crow, J. J. & Albig, A. R. Notch family members follow stringent requirements for intracellular domain dimerization at sequence-paired sites. *PLoS One* **15**, e0234101 (2020).

26. Liu, H. *et al*. Notch dimerization is required for leukemogenesis and T-cell development. *Genes Dev*. **24**, 2395–2407 (2010).

27. Siegel, R. L., Miller, K. D., Fuchs, H. E. & Jemal, A. Cancer statistics, 2022. *CA A Cancer J Clinicians* **72**, 7–33 (2022).

28. Sung, H. *et al*. Global Cancer Statistics 2020: GLOBOCAN Estimates of Incidence and Mortality Worldwide for 36 Cancers in 185 Countries. *CA A Cancer J Clin* **71**, 209–249 (2021).

29. Ganti, A. K. P. *et al*. Small Cell Lung Cancer, Version 2.2022, NCCN Clinical Practice Guidelines in Oncology. *Journal of the National Comprehensive Cancer Network* **19**, 1441–1464 (2021).

30. Bubendorf, L., Lantuejoul, S., de Langen, A. J. & Thunnissen, E. Nonsmall cell lung carcinoma: diagnostic difficulties in small biopsies and cytological specimens: Number 2 in the Series “Pathology for the clinician” Edited by Peter Dorfmüller and Alberto Cavazza. *Eur Respir Rev* **26**, 170007 (2017).

31. Chen, Z., Fillmore, C. M., Hammerman, P. S., Kim, C. F. & Wong, K.-K. Non-small-cell lung cancers: a heterogeneous set of diseases. *Nature Publishing Group* **14**, 535–546 (2014).

32. Thai, A. A., Solomon, B. J., Sequist, L. V., Gainor, J. F. & Heist, R. S. Lung cancer. *The Lancet* **398**, 535–554 (2021).

33. Ostrem, J. M., Peters, U., Sos, M. L., Wells, J. A. & Shokat, K. M. K-Ras(G12C) inhibitors allosterically control GTP affinity and effector interactions. *Nature* **503**, 548–551 (2013).

34. Camidge, D. R., Pao, W. & Sequist, L. V. Acquired resistance to TKIs in solid tumours: learning from lung cancer. *Nat Rev Clin Oncol* **11**, 473–481 (2014).

35. Cox, A. D. & Der, C. J. Ras history: The saga continues. *Small GTPases* **1**, 2–27 (2010).

36. Czernilofsky, A. P. *et al*. Nucleotide sequence of an avian sarcoma virus oncogene (src) and proposed amino acid sequence for gene product. *Nature* **287**, 198–203 (1980).

37. Czernilofsky, A. P. *et al*. Corrections to the nucleotide sequence of the src gene of Rous sarcoma virus. *Nature* **301**, 736–738 (1983).

38. Scolnick, E. M. & Parks, W. P. Harvey Sarcoma Virus: A Second Murine Type C Sarcoma Virus with Rat Genetic Information. *J Virol* **13**, 1211–1219 (1974).

39. Scolnick, E. M., Rands, E., Williams, D. & Parks, W. P. Studies on the Nucleic Acid Sequences of Kirsten Sarcoma Virus: a Model for Formation of a Mammalian RNA-Containing Sarcoma Virus. *J Virol* **12**, 458–463 (1973).

40. Willingham, M. C., Pastan, I., Shih, T. Y. & Scolnick, E. M. Localization of the src gene product of the Harvey strain of MSV to plasma membrane of transformed cells by electron microscopic immunocytochemistry. *Cell* **19**, 1005–1014 (1980).

41. Muñoz-Maldonado, C., Zimmer, Y. & Medová, M. A Comparative Analysis of Individual RAS Mutations in Cancer Biology. *Front. Oncol.* **9**, 1088 (2019).

42. Lau, K. S. & Haigis, K. M. Non-redundancy within the RAS oncogene family: Insights into mutational disparities in cancer. *Mol Cells* **28**, 315–320 (2009).

43. Moore, A. R., Rosenberg, S. C., McCormick, F. & Malek, S. RAS-targeted therapies: is the undruggable drugged? *Nat Rev Drug Discov* **19**, 533–552 (2020).

44. Trahey, M. & McCormick, F. A Cytoplasmic Protein Stimulates Normal N- *ras* p21 GTPase, But Does Not Affect Oncogenic Mutants. *Science* **238**, 542–545 (1987).

45. Hunter, J. C. *et al*. Biochemical and Structural Analysis of Common Cancer-Associated KRAS Mutations. *Molecular Cancer Research* **13**, 1325–1335 (2015).

46. Vasta, J. D. *et al*. KRAS is vulnerable to reversible switch-II pocket engagement in cells. *Nat Chem Biol* **18**, 596–604 (2022).

47. Hong, D. S. *et al*. KRAS ^{G12C} Inhibition with Sotorasib in Advanced Solid Tumors. *N Engl J Med* **383**, 1207–1217 (2020).

48. Awad, M. M. *et al*. Acquired Resistance to KRAS ^{G12C} Inhibition in Cancer. *N Engl J Med* **384**, 2382–2393 (2021).

CHAPTER 2

CHARACTERIZATION OF ENDOGENOUS PAN-NOTCH DEPENDENCE IN MOUSE AND HUMAN LUNG ADENOCARCINOMA MODELS

ABSTRACT

Though genetically engineered mouse models (GEMMs) are uniquely poised to study the contributions of cell intrinsic and extrinsic factors to tumorigenesis *in situ*, their capacity to conduct detailed mechanistic studies is limited by reproducibility, tissue availability and cost. Our previous findings established Notch3 as required for tumorigenesis in the Kras-p53 mouse LUAD model and our eventual aim is to study the global transcriptional activity of Notch3 in the lung cancer context. Here, we have generated cell lines derived from Kras-p53 mutant primary LUAD mouse tumors and assessed their pan-Notch dependency using chemical inhibitors. We find that spheroids from mouse cell lines demonstrate increased resistance to Notch inhibition, and that this recapitulates similar resistance observed in human LUAD cell lines. We conclude that both our mouse and human LUAD cell lines, despite transcriptional and protein-level evidence of Notch receptor expression, demonstrate limited dependence on activated Notch signaling and likely require either exogenous ligand-dependent activation or NICD expression to study downstream signaling activity.

INTRODUCTION

A potential role for Notch3 in lung cancer was first described over twenty years ago by Dang et al., who identified a highly aggressive and metastatic epithelial lung cancer in a non-smoking patient with a chromosomal 19 translocation resulting in the overexpression of Notch3[1]. Their report also discovered the same translocation in other non-small cell lung cancer cell lines, all with high expression of Notch3. Additional studies from the Rudin lab and others suggest that patient tumors with high Notch3 expression are also often high in EGFR expression, and that high Notch3 signaling allows "adaptive persister" cells to evade tyrosine kinase inhibitor-mediated cell death[2,3]. Expression of dominant negative Notch3 greatly impaired cell growth in serum-free but not complete media[4], which the authors postulated was due to a more rapid downregulation of ERK phosphorylation in the absence of Notch3 signaling. Interestingly, EGFR mutations dominantly suppress the notched wing mutant phenotype in *Drosophila*, suggesting a evolutionarily conserved link between the two signaling pathways[5].

Notch3 also generated significant interest because of its role in lung development. An early study expressing the Notch3 intracellular domain under the AT2-specific promoter SpC (surfactant protein C) was lethal *in utero* due to failure of embryonic lung development[6]. Upon investigation, the authors found that SpC-driven NICD3 expression led to failure of lung epithelial differentiation, metaplasia of the terminal airways, and complete loss of alveolar Type I cells. Later studies of proximal airway embryogenesis in knockout mice revealed that Notch3 is also required for maintenance of a progenitor parabasal population in a Jagged-dependent manner, while Notch1/2 drive secretory and ciliated cell fate adoption[7]. The role of Jagged in lung development was later confirmed by a seminal study which used Jagged1/2-blocking antibodies to demonstrate a loss of club cell lineage in favor of a ciliated cells through a non-

proliferative transdifferentiation phenotype[8], directly implicating Notch signaling as a regulator of cell fate in the adult lung as well as during development.

Efforts to define a role for Notch signaling in lung cancer has so far proven more elusive. Some early studies in $Kras^{G12D}$ LUAD mouse models suggested that Notch1 might be required for cell growth under hypoxic conditions[9] or to maintain p53 destabilization[10], and co-expression of Myc with constitutively activated Notch1 demonstrated much more rapid tumor growth than either oncogene expressed alone[11]. In the first demonstration of gamma-secretase inhibition (GSI) efficacy in the GEMM model, Maraver et al. reported that both genetic ablation of Rbpj as well as GSI monotherapy reduced overall tumor burden in the $Kras^{G12V}$ LUAD mouse model[12]. However, *in vivo* expression of dominant negative MAML failed to show any effect on lung tumorigenesis in the Kras-mutant GEMM[2], highlighting that not all methods of Notch inhibition are equal and reinforcing the importance of more refined and targeted methods such as, antibody-mediated blockade[8,13], to dissect regulation of Notch signaling. It is now more widely acknowledged that the individual Notch receptors show differences not only in cell type expression[14], but also in their regulation[15], ligand preferences[16–18] and non-canonical downstream signaling partners[19], though much of the receptor-specific differences remain unknown.

Our lab previously demonstrated in the $Kras^{G12D}$ $p53^{fl/fl}$ GEMM that tumor propagating capacity was greatly enriched in a CD24+ ITGB4+ Notch-hi cell population in which knockdown of Notch3, but not of the other Notch receptors, inhibited their *ex vivo* and *in vivo* proliferation[20]. A later study in LUAD cell lines identified a PKCγ-ELF3-NOTCH3 axis driving sphere formation and xenograft tumor growth through regulation of asymmetric cell division[21], suggesting that Notch3-mediated regulation of stemness features is preserved in the cell lines they examined. Here we examine the mouse and human LUAD cell lines for Notch receptor

expression and show that they demonstrate limited dependence on Notch signaling, suggesting that alternative methods such as co-culture with ligand-expressing cells, exogenous ligand stimulation or NICD expression is required to accurately model this complex signaling pathway.

RESULTS

Development and characterization of primary mouse cell line models

To generate cell lines from $Kras^{LSL\text{-}G12D}$ $p53^{fl/fl}$ mouse tumors, we initiated tumorigenesis in a cohort of KP and KPY (Cre-dependent YFP expression) mice through intratracheal instillation of Cre adenovirus and monitored the mice for development of symptoms indicative of tumor burden. Mice at endpoint were sacrificed and visible lung tumors were macrodissected before mincing and cells dissociated. After dissociation, the cell suspensions were filtered into single cells, depleted for immune-related lineage markers, and plated onto tissue culture dishes in standard cell culture medium. Cell lines from primary cells were passaged between 5-10 times to select out senescent fibroblasts and other non-tumor cell types before being banked at an early passage. The banked cell lines were used for these and future experiments, including the generation of rtTA-expressing cell lines (Chapter 3).

To assess whether the KP-derived cell lines maintained sphere-forming capacity, we plated single cell suspensions into Matrigel and imaged the resulting embedded spheroids by light and fluorescence microscopy (**Figure 2.1 A**). All primary cell lines continued to form spheres resembling those formed from newly dissociated tumor cells, though at a much faster rate (2-3 days vs. up to 7 days post-plating). We found that many, but not all of the resulting KPY spheres were YFP+, suggesting either incomplete recombination or the presence of non-tumor cells. We confirmed these findings by FACS from the 2D cell cultures, gating against the KP primary cell line in the FITC channel, which appeared to show anywhere from 7.5% YFP+ to >60% YFP+ cells in our two KPY cell lines (**Figure 2.1 B**). A third KPY cell line derived separately contained 24% YFP+ cells, reinforcing the heterogeneity of these models.

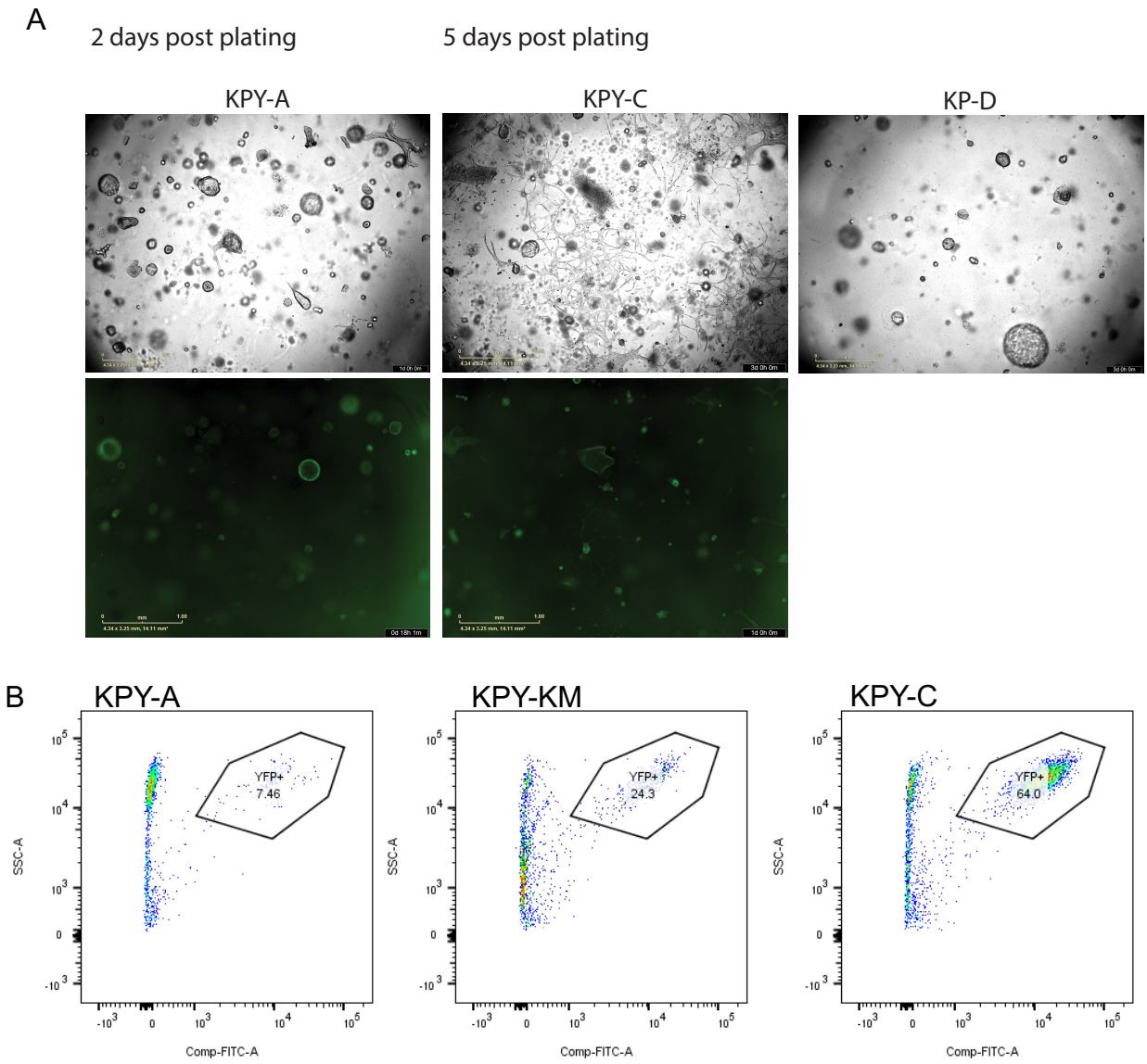

Figure 2.1 Development of primary cell line models derived from the Kras p53 mouse model.
A Light and fluorescent (GFP) images of primary cell taken 2 days (first column) and 5 days after plating.
B FACS plots of primary cell lines (2D culture) for YFP expression.

We further tested the cell line spheroids for sensitivity to three different gamma-secretase inhibitors, dibenzazepine (DBZ), DAPT (GSI-IX), and FLI-06, using puromycin as a positive control (**Figure 2.2 A**). FLI-06 (5 uM, EC50 of 2.3 uM) was unexpectedly as toxic as puromycin, possibly in an off-target manner. However, neither DAPT nor DBZ at their effective concentrations showed any effect on sphere viability after 5 days of treatment, suggesting that

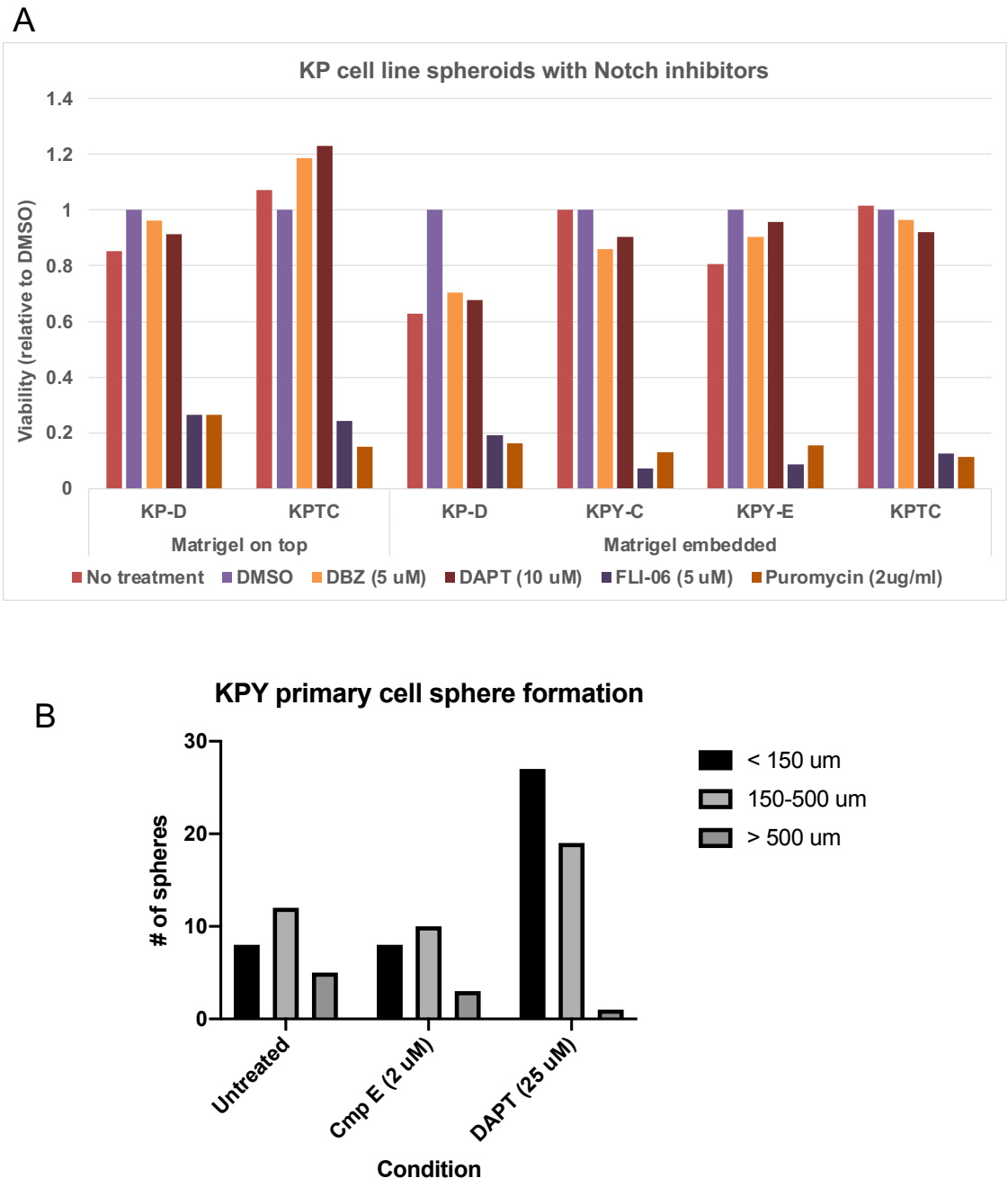

Figure 2.2 KP spheroids in culture and from primary tumors demonstrate limited viability response to Notch inhibitors. **A** Day 5 viability of KP cell line spheroids treated with Notch inhibitors (DBZ, DAPT, FLI-06) or a puromycin control. **B** KPY primary spheres treated with Notch inhibitors and measured 7 days after plating.

these cell line spheroids were insensitive to endogenous Notch inhibition. Unexpectedly, we found that treatment of KPY spheroids from primary cells (never cultured) with an even higher dose of DAPT or with Compound E, a GSI with the highest efficacy in cell culture, did not reduce the total number of spheres, though DAPT did appear to inhibit the formation of very large spheres greater than 500 μm in diameter (**Figure 2.2 B**). From these data, we concluded that neither the cell line-derived nor primary tumor spheroids demonstrated *in vitro* dependence upon pan-Notch signaling.

Human lung adenocarcinoma cell lines are not dependent on endogenous Notch activity

We then turned to assess Notch inhibitor sensitivity in human lung adenocarcinoma cell lines. CCLE RNA-seq data of all LUAD cell lines suggested that the majority (9/13) express Notch3 at or above a threshold of 2 RPKM ("High"), while one and three cell lines demonstrated moderate to low Notch3 expression, respectively (**Figure 2.3 A**). Western blot analysis of Notch receptor protein expression in available cell lines corresponded relatively well with transcript expression (**Figure 2.3 B**), including the three low Notch3 cell lines (H23, H1299, H1975), but with the exception of H441, which had relatively high Notch1 and Notch2 protein expression but low Notch3 protein expression, in contrast to transcript data suggesting Notch2 = Notch3 > Notch1.

A

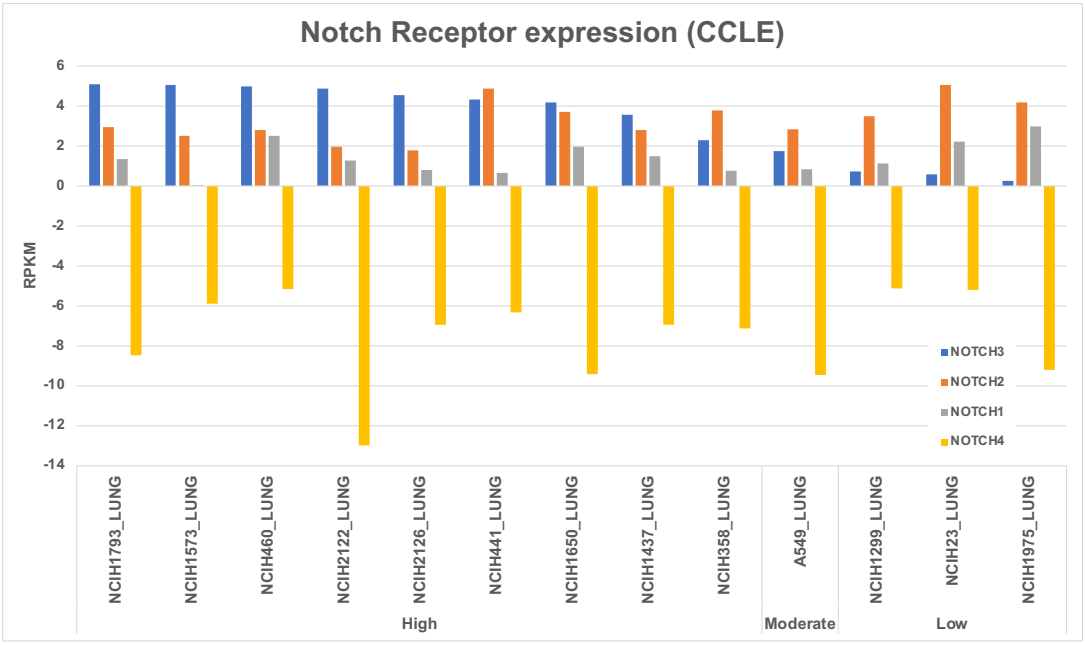

B

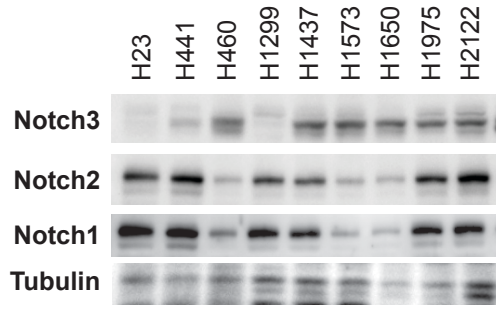

C

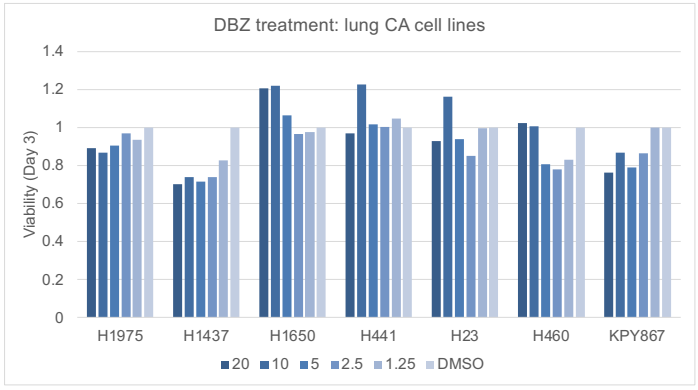

Figure 2.3 Notch receptor expression in a panel of human LUAD cell lines. A CCLE expression data of Notch receptors in human lung adenocarcinoma (LUAD) cell lines. **B** Western blot for Notch receptor expression in human LUAD cell lines. **C** Viability (Alamar Blue) of LUAD cell lines after Day 3 of DBZ treatment.

A panel of these cell lines, including a KPY line (previously KPY-D, hence referred to as KPY867) were plated in increasing doses of the gamma-secretase inhibitor DBZ and assessed at day 3 post-treatment by Alamar Blue, a resazurin-based viability assay (**Figure 2.3 C**). Only viability data from two cell lines, H1437 and KPY867, demonstrated a dose-dependent response to DBZ, while the others showed inconsistent (H460) or no change from DMSO control. Growth kinetics and additional timepoints were analyzed using Incucyte cell confluence data (**Figure 2.4**). By day 5 of DBZ treatment (0.63-10 uM), H441, H1437, and H2122 growth rates slowed in a dose-dependent manner, while H1650 and H1537 did not (**Figure 2.4**). To assess whether Notch inhibition might suppress anchorage-independent colony formation, we plated the LUAD cell lines into methylcellulose and treated with a higher dose range of DBZ (1.25-20 uM) for seven days (**Figure 2.5**). Paradoxically, all cell lines capable of colony formation appeared to show a dose-dependent increase in sphere growth (analyzed as area confluence) in response to DBZ. The rationale for this finding remains unclear, though one possibility is that Notch receptor-ligand interactions in 3D culture might function to restrict growth in a relatively nutrient-depleted environment.

Finally, we asked whether Notch signaling, specifically through Notch3, might be more strongly inhibited in the GSI-sensitive cell lines as compared to the GSI-insensitive cell lines. We chose H1437 and H441 as our most sensitive cell lines and H1650 as our resistent cell line, and first assessed whether we could detect the loss of the Notch3 intracellular domain (NICD3) by Western blot using antibodies developed against the C-terminal domain of Notch3. In these and two other cell lines with moderate GSI sensitivity (H1573 and H2126), we found that we were able to detect full-length/transmembrane Notch3 (~200 kDa) and the post-S2 membrane-bound NEXT fragment (~90 kDa). We observed GSI-dependent accumulation of the full-

length/TM Notch3 receptor with one antibody, while the NEXT fragment detected by the second antibody appeared unchanged (**Figure 2.6 A**). Neither commercially available antibody, nor a panel of other antibodies tested, were able to detect the NICD3 fragment, which would be expected to appear as a band of around 80 kDa that is lost upon GSI treatment (**Figure 2.7**). We also confirmed that GSI treatment was downregulating Notch-dependent targets through qPCR expression analysis of Hes1, Hes5, Hey1 and Hey2 as expressed (**Figure 2.6 B**). A transient "release" into serum-containing media also assessed the extent to which Notch signaling could acutely recover after GSI treatment, and this revealed that the "resistant" cell line (H1650) recovered expression of Notch targets more rapidly than the "sensitive" cell lines. This was unexpected because the H1650 cell line comparatively expressed the lowest amount of the receptors, including Notch3, by Western, but could be potentially be explained by the frequent degredation and recycling of cleaved receptor/ligand products.

DISCUSSION

Historically, Notch signaling and its regulation of cell fate has been studied using model organisms that permitted genetic manipulation and precise tracking of tissue development. Since the discovery of Notch1 mutations in leukemia[22], alterations in the Notch pathway in tumorigenesis have been the subject of intense investigation over the past several decades, yet if anything, the majority of research (with a few notable exceptions) has led to conflicting models between cell lines, mouse models, and patient data. This is likely driven by the inherent complexity of Notch-mediated signaling, which is under exquisite control during development and mediates many of its downstream effects in a cell context-specific manner.

Here, we explored the effect of gamma-secretase inhibition in mouse and human lung adenocarcinoma cell lines, with the intention of ultimately studying transcriptional activity mediated by Notch epigenetic regulation. We find that despite robust Notch receptor and target expression in our cell lines, these exhibit limited dependency on Notch signaling, suggesting that the study of endogenous transcriptional activity would likely yield unclear or insignificant results. We did not study ligand-induced transcriptional signaling, as it is yet unclear what ligands are relevent to the lung tumor context other than one report that Jagged2 can promote EMT and metastasis in LUAD[23]. Relying on commericially purchased ligands would be cost-prohibitive for our mechanistic studies, but validation with either a heterotypic ligand-activated cell line model or an *in vivo* model of Notch activation is important for understanding the generalizability of our models and prioritizing targets that are required for Notch-dependent effects on tumor cell proliferation and stemness.

Interestingly, it is thought that KRAS activation may reduce the sensitivity of NSCLC to gamma-secretase inhibition, as knockdown of the mutant KRAS allele sensitized cell lines to GSIs[24]. This is consistent with our data which suggest that the most "sensitive" cell line harbors no RTK pathway mutations, while the second-most GSI-responsive cell line harbors an EGFR activating mutation and wildtype KRAS. Other studies have shown that GSI has moderate effect on clonogenic survival and tumor growth *in vivo*, but most reproducibly alters growth in a serum-depedent manner[25]. This, together with data that genetic Notch1 ablation suppress cell growth under hypoxic conditions[9], suggests that the pan-Notch signaling may most likely be required to maintain cell survival under stress rather than proliferation in nutrient-rich conditions.

One of the few advantages of cell lines over EGFR- and KRAS-driven genetically engineered mouse models (GEMM) is that these often have a far lower mutational burden than either NSCLC patients or even LUAD GEMMs driven by weaker oncogenes, such as Myc[26]. Thus, patient-derived cell lines are capable of modeling the genetic heterogenity more closely, perhaps, than mouse primary spheroids or cell lines, and this may explain part of the resistance to GSIs. Alternatively, we propose that Notch may not be required for cell survival or proliferation, but rather contribution to lung tumor progression in a transient manner, and that by studying the relevent downstream effectors of Notch, we will be able to more broadly identify the pathways involved in tumor development and design better models for understanding this disease.

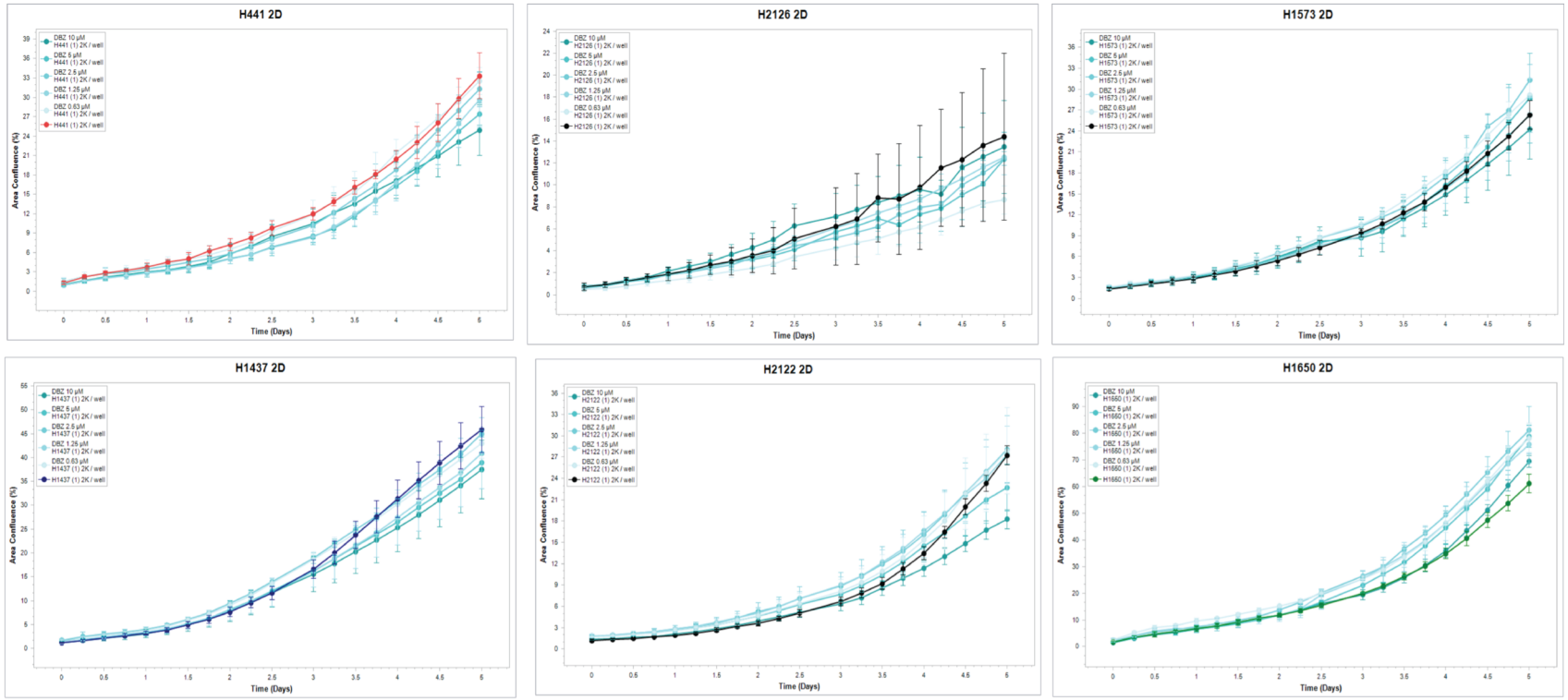

Figure 2.4 Area confluence of human LUAD cell lines in 2D with DBZ gamma-secretase inhibitor for 7 d
Each point represents the average of three well replicates which are normalized to day 0.

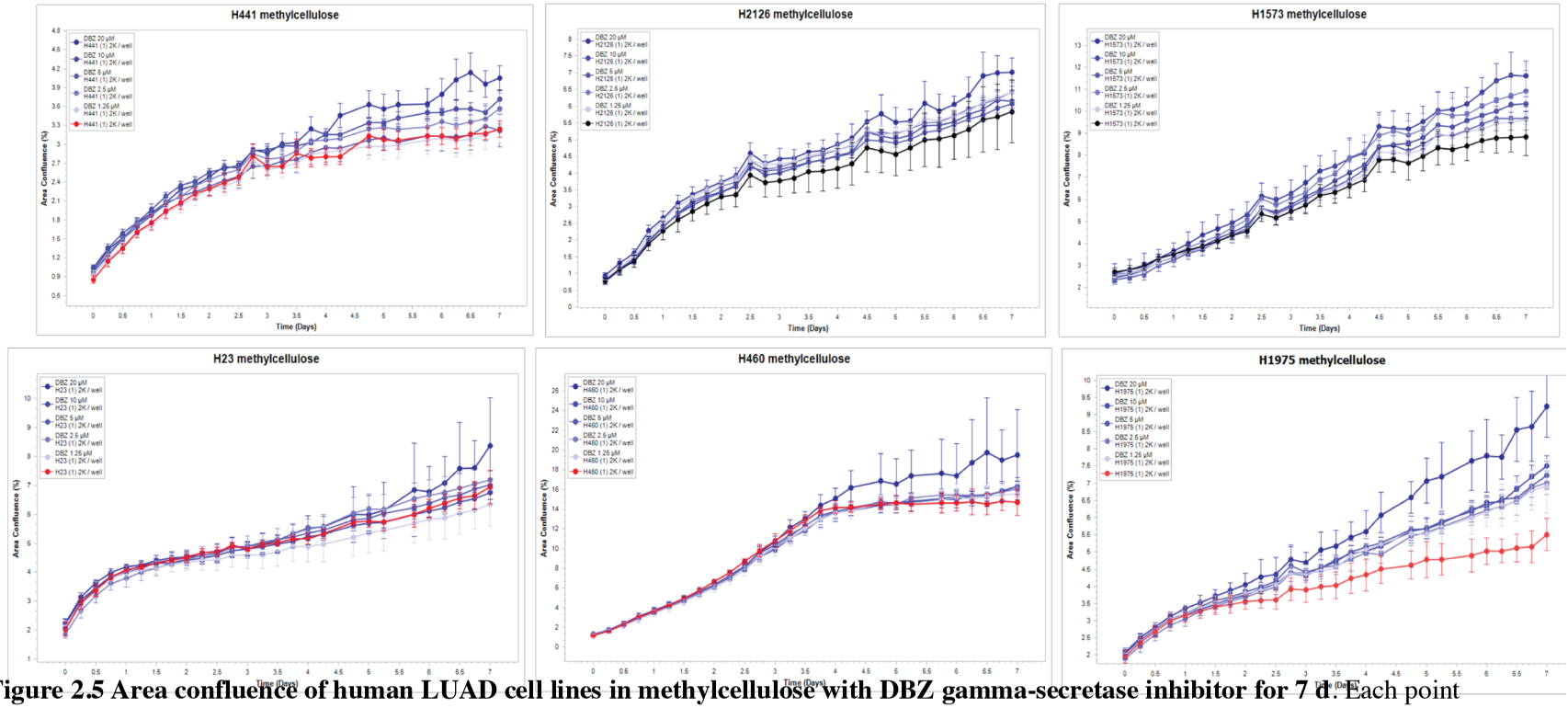

Figure 2.5 Area confluence of human LUAD cell lines in methylcellulose with DBZ gamma-secretase inhibitor for 7 d. Each point represents the average of three well replicates which are normalized to day 0**.**

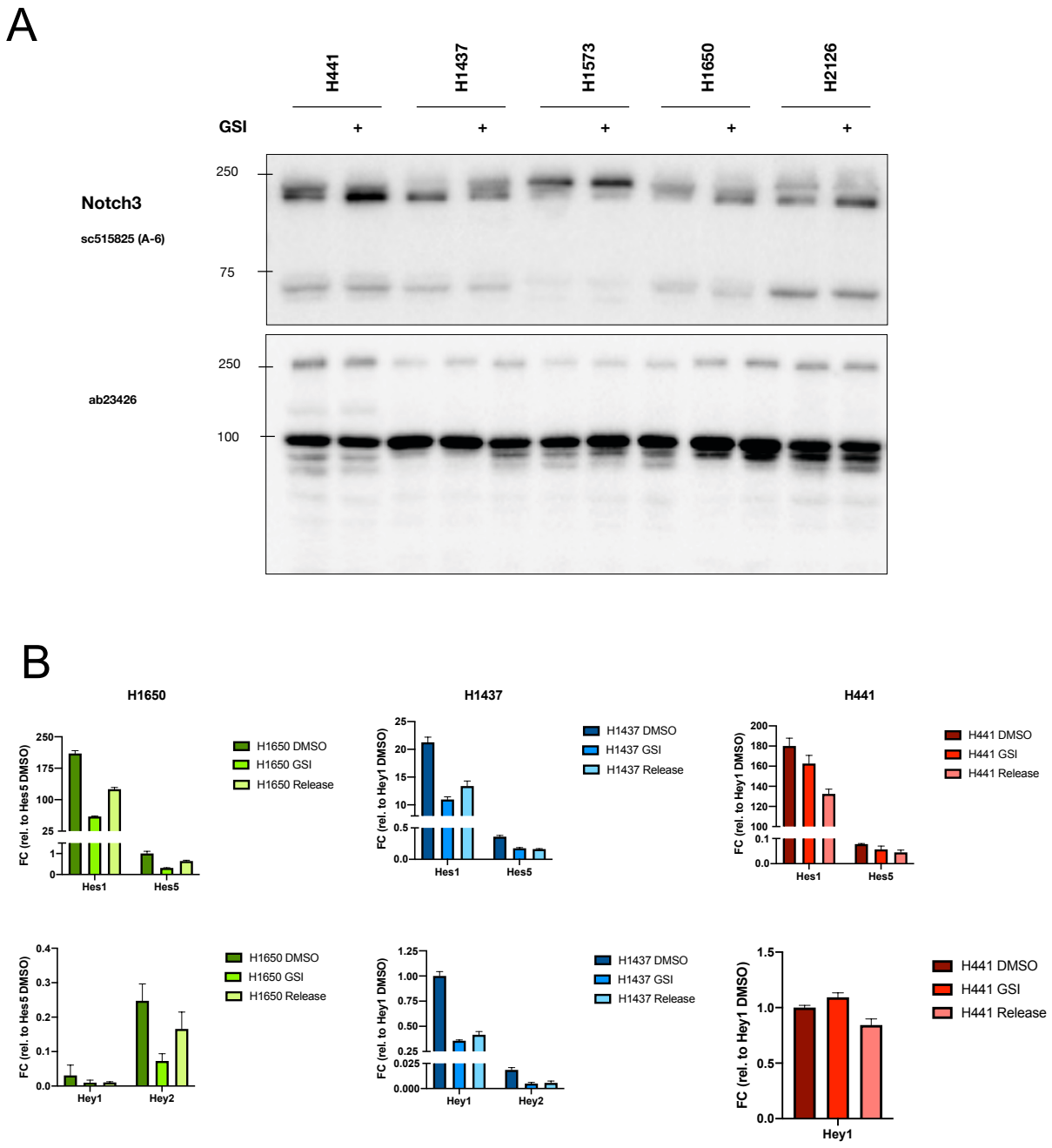

Figure 2.6 Human LUAD cell line responsivity to Notch inhibition. A Western blot of Notch3 in human LUAD cell lines demonstrating accumulation of full length NICD after 48 h of GSI treatment. **B** Gene expression changes of Notch targets Hes1, Hes5, Hey1, and Hey2 after GSI treatment (72 h) with or without release into serum (4 h). Hey2 was not detected in the H441 cell line.

MATERIALS AND METHODS

GEMM LUAD models and cell line derivation

In vivo studies were conducted under University of California San Francisco's Institutional Animal Care and Use Committee (IUCAC) approved protocol (Protocol # AN182332-03I) in accordance with approved guidelines. To initiate tumor formation, 4-6 month-old $Kras^{LSL\text{-}G12D}$ $p53^{fl/fl}$ and $Kras^{LSL\text{-}G12D}$ $p53^{fl/fl}$ YFP mice were administered intranasally with Cre adenovirus as previously described[20]. Mice were monitored for tumor burden and sacrificed at endpoint as determined by protocol guidelines. Visible tumors were macrodissected, minced, and dissociated in 10 ml of dissociation media (DMEM/F20, 1 U/ml DNase, collagenase/dispase) at 37C with shaking for 1 h. The cell suspension was filtered twice through 40 uM filters prior to red blood cell lysis. After resuspension in PBS with 10% bovine growth serum (Hyclone), lineage depletion of immune and RBC markers were performed using CD34, CD45, and Ter-119 antibodies (Biolegend). The remaining cells were counted by hemocytometer and either used for primary spheroid assays or plated onto standard TC-coated dishes for cell line generation.

Cell culture and Reagents

The human lung cancer cell lines H23, H441, H460, H1299, H1437, H1573, H1650, H1975, and H2122 were purchased from ATCC. KP and KPY cell lines were derived from primary mouse lung adenocarcinoma tumors as described. Human cell lines were cultured in RPMI1640 medium (Corning 17-105-CV) and KPY-867 in DMEM (Corning 15-103-CV). Base media was supplemented with 10% fetal bovine serum (Hyclone) and 1% penicillin-streptomycin-glutamine (Gibco), and all cell lines were cultured in a humidified CO_2 incubator at 37C. Human cell lines were authenticated by STR profiling and all cell lines were routinely tested for mycoplasma.

DAPT, DBZ, and FLI-06 were purchased from Selleck Chemicals. Compound E was purchased from MilliporeSigma.

3D spheroid cultures

To generate primary and cell line-derived spheroids, 500 to 1000 cells were plated in stem cell media (DMEM/F20, 10% FBS, 1% pen-strep, EGF/FGF, bovine pituitary extract) with 50% phenol-red free Matrigel (Corning #356237) in 96-well format and allowed to set for 30 min before adding stem cell media with or without drug, for treatment assays. Spheroids were imaged on an inverted fluorescent microscope (Leica) beginning at 2 days (cell line) and 7 days (primary cells) after plating. Spheroid viability after drug treatment was measured using alamarBlue as described below.

Flow cytometry

KPY cell lines were harvested into trypsin, resuspended into complete DMEM medium, and filtered into single cell suspensions. YFP expression of single cells was analyzed on a BD Accuri.

Viability assays

1000-5000 cells per well were plated into clear-bottomed 96-well plates (Corning #353072) and incubated overnight. The next day, drug treatments were added at the indicated concentrations and plate confluence read by Incucyte imaging analysis through day 7 post-treatment. For the methylcellulose assays, 500-1000 cells were resuspended in 2% methylcellulose in complete RPMI medium, incubated, and treated the next day before initiating imaging. For viability plates read by colorimetric analysis, cells were plated and treated as above. At three days post-treatment, cells were incubated for 4h with alamarBlue (Invitrogen) at 37C and absorbance read at 570 nm on a plate reader (BioTek).

Antibodies and Western blotting

Cultured cells for protein analysis were directly scraped into ice-cold PBS, resuspended in RIPA lysis buffer (Sigma) supplemented with protease and phosphatase inhibitors (Pierce), and lysed on ice for 30 min. Lysates were clarified at 16,000xg for 10 min, quantified by BCA assay (Pierce), and reduced in 6X Laemelli sample buffer for 20 min at 72C prior to loading on 10% Tris-Glycine gels. Gels were transferred to PVDF membranes at 100V for 90 min, blocked for 1 h in 5% dry milk in TBST (w/v), and incubated overnight at 4C with the following primary antibodies: Notch1 (Cell Signaling #3608), Notch2 (Cell Signaling #5732), Notch3 (Cell Signaling #5276), alpha-Tubulin (Sigma, T6199), Notch3 (Abcam, ab23426), and Notch3 (Santa Cruz, sc-515825). The next day, blots were washed three times in TBST and incubated with secondary antibody in milk (Jackson Immunoresearch, 1:5000 for rabbit and 1:2500 for mouse) for 1 h at room temperature before visualization with Clarity Western ECL Substrate (BioRad) or SuperSignal (Pierce). Blots were imaged on the ChemiDoc Imaging system (BioRad).

Quantitative real-time PCR

100-500,000 untreated cells were plated into 6-wells, treated with drug as indicated, and harvested into TRIzol (Invitrogen). Total RNA was isolated using the Direct-zol RNA kit (Zymo) and quantified by Nanodrop. cDNA was synthesized from 1 ug of purified RNA using the Maxima First Strand cDNA synthesis kit (Thermo Scientific) and qPCR was performed using PerfeCta SYBR Green SuperMix (Quanta Biosciences) on a BioRad CFX96 real-time PCR detector. qPCR primer sequences for human Hes1, Hes5, Hey1 and Hey2 were adapted from Xiao et al[27].

REFERENCES

1. Dang, T. P. *et al*. Chromosome 19 Translocation, Overexpression of Notch3, and Human Lung Cancer. *JNCI Journal of the National Cancer Institute* **92**, 1355–1357 (2000).

2. Osanyingbemi-Obidi, J., Dobromilskaya, I., Illei, P. B., Hann, C. L. & Rudin, C. M. Notch Signaling Contributes to Lung Cancer Clonogenic Capacity In Vitro but May Be Circumvented in Tumorigenesis In Vivo. *Molecular Cancer Research* **9**, 1746–1754 (2011).

3. Arasada, R. R. *et al*. Notch3-dependent b-catenin signaling mediates EGFR TKI drug persistence in EGFR mutant NSCLC. *Nature Communications* 1–16 (2018) doi:10.1038/s41467-018-05626-2.

4. Konishi, J. *et al*. Notch3 cooperates with the EGFR pathway to modulate apoptosis through the induction of bim. *Oncogene* **29**, 589–596 (2009).

5. Price, J. V., Savenye, E. D., Lum, D. & Breitkreutz, A. Dominant Enhancers of *Egfr* in *Drosophila melanogaster:* Genetic Links Between the *Notch* and *Egfr* Signaling Pathways. *Genetics* **147**, 1139–1153 (1997).

6. Dang, T. P., Eichenberger, S., Gonzalez, A., Olson, S. & Carbone, D. P. Constitutive activation of Notch3 inhibits terminal epithelial differentiation in lungs of transgenic mice. *Oncogene* **22**, 1988–1997 (2003).

7. Mori, M. *et al*. Notch3-Jagged signaling controls the pool of undifferentiated airway progenitors. *Development* **142**, 258–267 (2015).

8. Lafkas, D. *et al*. Therapeutic antibodies reveal Notch control of transdifferentiation in the adult lung. *Nature Publishing Group* **528**, 127–131 (2015).

9. Chen, Y. *et al*. Oxygen Concentration Determines the Biological Effects of NOTCH-1 Signaling in Adenocarcinoma of the Lung. *Cancer Research* **67**, 7954–7959 (2007).

10. Licciulli, S. *et al*. Notch1 Is Required for Kras-Induced Lung Adenocarcinoma and Controls Tumor Cell Survival via p53. *Cancer Research* **73**, 5974–5984 (2013).

11. Allen, T. D., Rodriguez, E. M., Jones, K. D. & Bishop, J. M. Activated Notch1 Induces Lung Adenomas in Mice and Cooperates with Myc in the Generation of Lung Adenocarcinoma. *Cancer Research* **71**, 6010–6018 (2011).

12. Maraver, A. *et al*. Therapeutic effect of γ-secretase inhibition in KrasG12V-driven non-small cell lung carcinoma by derepression of DUSP1 and inhibition of ERK. *Cancer Cell* **22**, 222–234 (2012).

13. Wu, Y. *et al*. Therapeutic antibody targeting of individual Notch receptors. *Nature* **464**, 1052–1057 (2010).

14. Raafat, A. *et al*. Expression of Notch receptors, ligands, and target genes during development of the mouse mammary gland. *J. Cell. Physiol.* **226**, 1940–1952 (2011).

15. Groot, A. J. *et al*. Regulated Proteolysis of NOTCH2 and NOTCH3 Receptors by ADAM10 and Presenilins. *Molecular and Cellular Biology* **34**, 2822–2832 (2014).

16. Morimoto, M., Nishinakamura, R., Saga, Y. & Kopan, R. Different assemblies of Notch receptors coordinate the distribution of the major bronchial Clara, ciliated and neuroendocrine cells. *Development* **139**, 4365–4373 (2012).

17. Van de Walle, I. *et al*. Specific Notch receptor–ligand interactions control human TCR-αβ/γδ development by inducing differential Notch signal strength. *J Exp Med* **210**, 683–697 (2013).

18. Nandagopal, N. *et al*. Dynamic Ligand Discrimination in the Notch Signaling Pathway. *Cell* **172**, 869-880.e19 (2018).

19. Elyaman, W. *et al*. Notch Receptors and Smad3 Signaling Cooperate in the Induction of Interleukin-9-Producing T Cells. *Immunity* **36**, 623–634 (2012).

20. Zheng, Y. *et al*. A Rare Population of CD24+ITGB4+Notchhi Cells Drives Tumor Propagation in NSCLC and Requires Notch3 for Self-Renewal. *Cancer Cell* **24**, 59–74 (2013).

21. Ali, S. A., Justilien, V., Jamieson, L., Murray, N. R. & Fields, A. P. Protein Kinase C lambda Drives a NOTCH3-dependent Stem-like Phenotype in Mutant KRAS Lung Adenocarcinoma. *Cancer Cell* **29**, 367–378 (2016).

22. Aster, J. C., Pear, W. S. & Blacklow, S. C. Notch Signaling in Leukemia. *Annu. Rev. Pathol. Mech. Dis*. **3**, 587–613 (2008).

23. Yang, Y. *et al*. The Notch ligand Jagged2 promotes lung adenocarcinoma metastasis through a miR-200–dependent pathway in mice. *Journal of Clinical Investigation* **121**, 1373–1385 (2011).

24. Morgan, K. M. *et al*. Gamma Secretase Inhibition by BMS-906024 Enhances Efficacy of Paclitaxel in Lung Adenocarcinoma. *Molecular Cancer Therapeutics* **16**, 2759–2769 (2017).

25. Konishi, J. *et al*. γ-Secretase Inhibitor Prevents Notch3 Activation and Reduces Proliferation in Human Lung Cancers. *Cancer Research* **67**, 8051–8057 (2007).

26. McFadden, D. G. *et al*. Mutational landscape of EGFR-, MYC-, and Kras-driven genetically engineered mouse models of lung adenocarcinoma. *Proceedings of the National Academy of Sciences* **113**, E6409–E6417 (2016).

27. Xiao, Y. *et al*. The lymphovascular embolus of inflammatory breast cancer exhibits a Notch 3 addiction. *Oncogene* **30**, 287–300 (2011).

CHAPTER 3

CHARACTERIZATION OF THE NOTCH3-INDUCED CELL STATE IN LUNG ADENOCARCINOMA

ABSTRACT

Tumor heterogeneity manifests in both cell intrinsic and extrinsic forms, where the former encompasses genetic and epigenetic variation while the latter relies upon niche-dependent factors such as between tumor and stroma. From a disease perspective, such heterogeneity is advantageous because it allows for adaptation under diverse selective pressures including anchorage independence and metastasis. From a therapeutic perspective, the contribution of heterogeneity to resistance has long been recognized: most common cytotoxic treatment modalities eliminate rapidly dividing cells while leaving a reservoir of resistant clones prone to future relapse. This is particularly applicable to cancers diagnosed at later stages, as is common for lung cancer where 80% of patients present with advanced, non-localized disease and the five-year survival rate remains a dismal 20%. Therefore, it is essential to understand what drives survival and proliferation of clones with high tumorigenic and chemoresistant properties.

We previously reported the role of Notch3 in the maintenance of self-renewal properties in the GEMM model of lung adenocarcinoma. Here, we utilize transcriptomic and epigenomic analyses of Notch3-intraceullar domain (NICD3)-expressing LUAD cell lines to investigate the potential mechanisms by which this occurs. We show that Notch3-dependent transcriptional signature regulates Rho GTPase pathway effectors and lung lineage-specifying genes. We further demonstrate that Notch3 promotes the epithelial-to-mesenchymal transition (EMT) in Kras-mutant LUAD cell lines, and that this underlies Notch-driven resistance to Kras G12C inhibition. Our work nominates Notch3 as a potential driver of tumor progression and therapeutic resistance, and defines a subset of direct Notch3 target genes which likely modulate these phenotypes.

INTRODUCTION

The cancer stem cell (CSC) hypothesis postulates that, as in normal development, tumor development occurs in a hierarchical manner from a subset of "stem cells" capable of both self-renewal[1]. In the classic model, CSCs (also called "tumor-propagating cells", or TPCs, in the context of solid tumors) are thought to give rise to an intermediary transit-amplifying population which will eventually reach terminal differentiation and no longer divide (**Figure 3.1**). In contrast, a stochastic model suggests that TPCs and "differentiated" cells can freely interconvert between self-propagating and amplifying states, without an irreversible hierarchy[2]. Lineage tracing experiments using GEMMs to track clonal proliferation in multiple cancer types have revealed that a subset of definable clones may drive clonal expansion, giving rise to cells with limited proliferative capacity[3,4], while other studies have isolated highly tumorigenic cells *ex vivo* from primary patient tumors[5,6]; however, a direct relationship in clinical tumor evolution is far more challenging to demonstrate.

Though any number of putative stemness markers have been published, with varying degrees of evidence, for both primary human tumors and mouse models, the majority of these enrich for TPC-like behavior rather than demonstrating a direct contribution to tumorigenesis[7]. In addition, a number of caveats hinder the generalizability of such studies, including the limited capacity to identify cell states based on the selection of known surface markers. Another complicating factor is the contribution of the tumor microenvironment, as it has been shown that hypoxic and nutrient-deprived conditions may also promote a self-renewal state[1].

Despite the uncertainty surrounding the precise identity and contribution of TPCs, there is evidence that certain pathways are recurrently utilized, and perhaps required, for cancers of particular developmental origins. For example, when Lgr5+ cells in colorectal cancer patient-

derived and GEMM tumors and are ablated, differentiated cell types are able to rederive the Lgr5+ population, suggesting that the Lgr5+ state is necessary for tumor progression, if not tumor initiation, even if only in a transient manner[8,9]. In LUAD, single cell data from primary patient tumors and adjacent normal lung tissue revealed the existence of tumor cells with mature lineage lung signatures (alveolar type I, II, club, and ciliated cell types) and other with mixed lineage signatures along a developmental continuum driven by SOX2 and SOX9, both key regulators of normal lung embryogenesis[10]. Intriguingly, both the authors' identified "quiescent" stem-like state and hyperproliferative SOX9+ cell state upregulated MHC class I markers, required for evading Natural Killer cell-mediated clearance, while the SOX2+ regenerative cell type did not, suggesting that these lineages had an advantage during metastatic escape in circulation. Elimination of the NK cell population in an orthotopic model of lung metastasis revealed enrichment of SOX2+ cells, supporting the hypothesis that a so-called terminal cell state may harbor non-cell intrinsic advantages. This observation, coupled with evidence for tumor cell plasticity, makes clear why it is important to study the cell states themselves, as a transient or reversible state necessary for tumor progression may not be evident from a single snapshot of its developmental trajectory.

We previously demonstrated that Notch3 has a role in promoting the self-renewal of mouse lung cancer primary cells, nominating a role for Notch3 in maintenance of a stem-like program in LUAD; however, very little is known about the actual downstream mechanism of Notch3 activity. In this study, we interrogate the transcriptional and epigenetic consequences of Notch3-intracellular domain (NICD3) expression in the KRAS-mutant lung adenocarcinoma context using a tagged expression system in human cell lines. We find that Notch3 transcriptionally regulates growth factor-related signaling pathways and lung linage-specifying

genes, promoting cells towards a less differentiated state. We report that Notch3 binding is highly enriched at the promoters of Rho family genes, a pathway which has been recently been reported to modulate anti-EGFR therapy resistance and cell lineage in LUAD[11]. Finally, we demonstrate a role for NICD3 in the induction of EMT, tumor progression, and therapeutic resistance to KRAS(G12C) inhibition. We propose that NICD3 contributes to stemness in LUAD through modulation of the EMT phenotype and importantly, that this suggests that Notch activity may be responsible for intrinsic resistance phenotypes observed in recent clinical trials of covalent KRAS(G12C) small molecule inhibitor monotherapies.

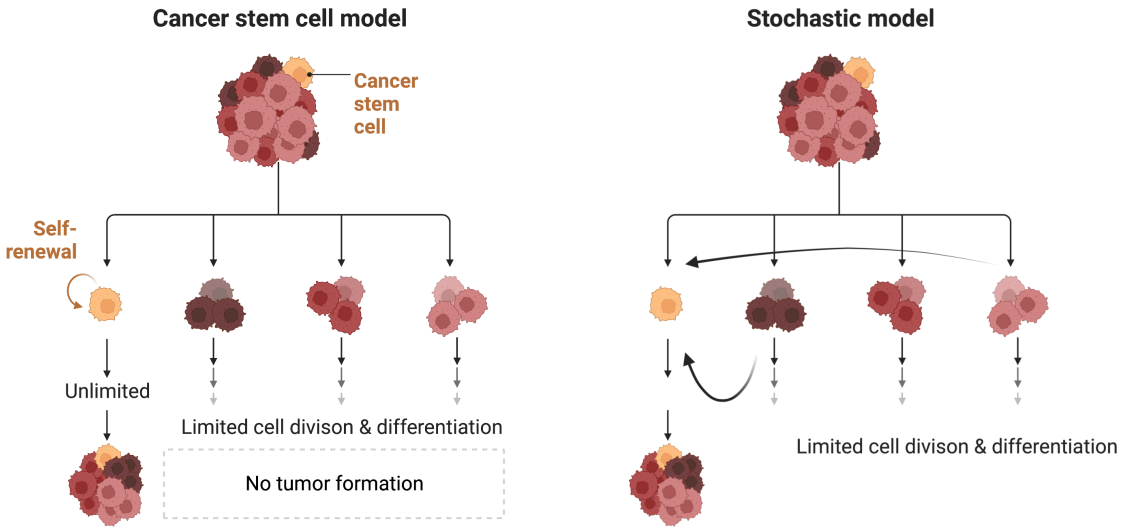

Figure 3.1 Models of cancer stemness. The hierarchical cancer stem cell model (left) posits that only certain tumor cells retain the capacity for self-renewal, and these cells are capable of differentiating into terminal subtypes. In contrast, the stochastic model suggests that even so-called "terminal" cells may, under the right environmental circumstances, transit into a self-renewing cell state. This phenotypic switch is called cancer cell plasticity. Figure generated with Biorender.

RESULTS

Generation of lung adenocarcinoma cell lines with inducible Notch3-intracellular domain

To study the genome-wide transcriptional activity of Notch3 in lung adenocarcinoma, we engineered an doxycycline-dependent model[12] (**Figure 3.2**) to inducibly express a V5-tagged Notch3 intracellular domain (NICD3-V5) which, when expressed on its own, acts constitutively as a transcriptional co-regulator in conjunction with transcription factors such as Rbpj[13]. We expressed either NICD3-V5 or a luciferase-V5 control[14] in both mouse (KPY867) and human cell line models (H441, H358, H1573, H1437) (**Table 3.1**).

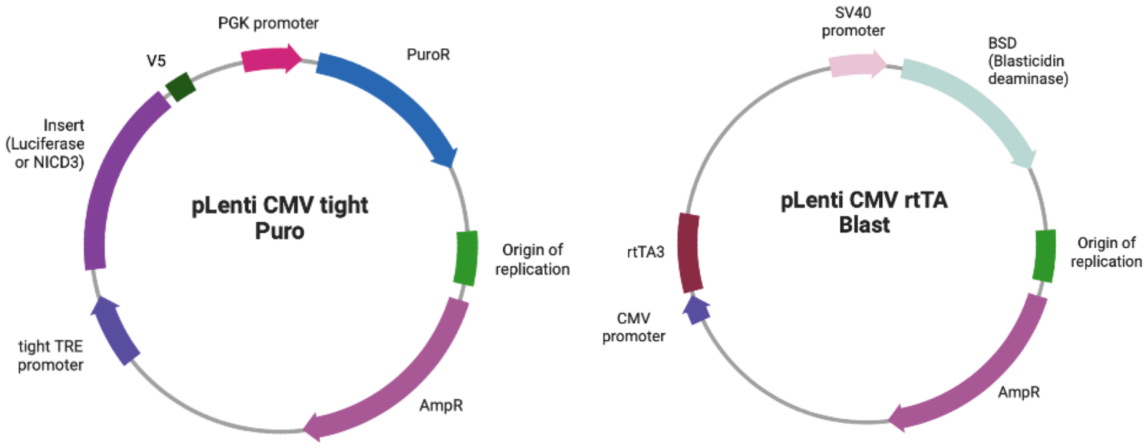

Figure 3.2 Plasmid maps of vectors used to generate inducible cell lines. (Left) Expression vector with CMVtight TRE promoter used to express a V5-tagged insert. (Right) Third-generation rtTA-expression vector used to generate stable rtTA cell lines. (Figure generated with Biorender.)

The KPY867 and H1437 cell lines were initially chosen for their relative sensitivity to Notch inhibition compared to the other lung cancer cell lines, as described previously. Upon expressing NICD in these two cell lines, we discovered the KPY867, but not the H1437 cell line, underwent a striking phenotypic change from the parental, adherent epithelial sheets into aggregative, detached cells with spindly appearance (**Figure 3.3**). Given that the KPY867 cell

Table 3.1 Select human LUAD cell lines with Kras/TP53 mutation status.
Cell lines are classified as "epithelial" or "mesenchymal" using a ratio of log-fold change E-cadherin: log-fold change Vimentin > 2 (Expression values from CCLE RNA-seq dataset).

	Kras status	TP53 status	VIM expression	E-Cadherin expression	Ecad/Vim LFC Ratio	
H358	G12C (heterozygous)	del	5.19	6.67	2.79	Epi
H23	G12C (heterozygous)	p.M246I	8.54	3.70	0.04	Mes
H1792	G12C (homozygous)	c.672+1G>A (splice donor)	8.67	0.76	0.00	Mes
H2122	G12C (homozygous)	p.G16L/C176F	-1.06	4.16	37.33	Epi
H441	G12V (homozygous)	p.R158L	0.41	7.12	105.00	Epi
H1437	wildtype	p.R267P	-0.89	5.38	76.98	Epi
H1573	G12A (heterozygous)	p.R248L	-1.28	7.35	394.81	Epi

line was derived from tumors initiated with the Kras-G12D p53 mutations and that H1437 cells were Kras wildtype, we hypothesized that we might observe similar phenotypic changes in Kras mutant human cell lines. Consequently, we chose to further characterize NICD3 expression in KPY867, H441 and H358 as representative epithelial cell lines (defined by a log-fold change ratio of E-cadherin:Vimentin > 2) with activating Kras mutations (**Table 3.1**). To note, all cell lines harbored TP53 mutations as typical of the majority of LUAD cell lines.

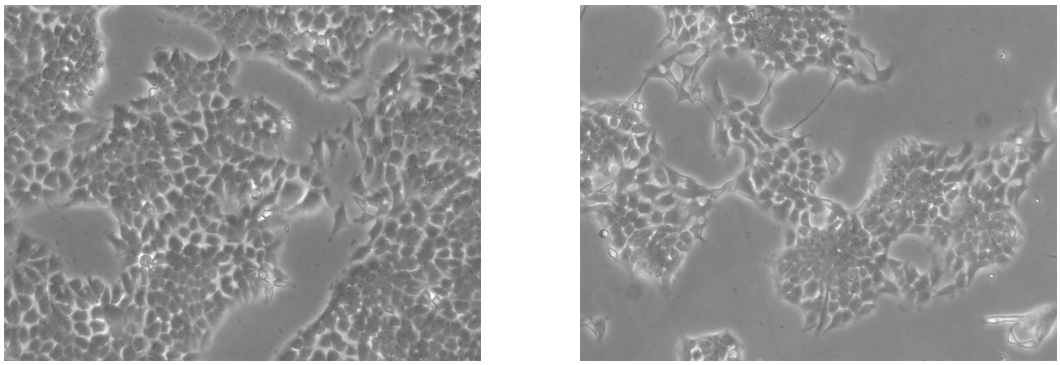

Figure 3.3 Light micrographs of KPY867 NICD cells. Cells cultured on TC-treated dishes and imaged at 40X magnification. (Left) Naive (no dox) KPY867-NICD cells. (Right) KPY867-NICD cells after 96 h of doxycycline.

All cell lines demonstrated robust V5 expression in response to 48 h of doxycycline with minimal leakiness, as well as upregulation of the canonical Notch target Hey1 (**Figure 3.4**). In

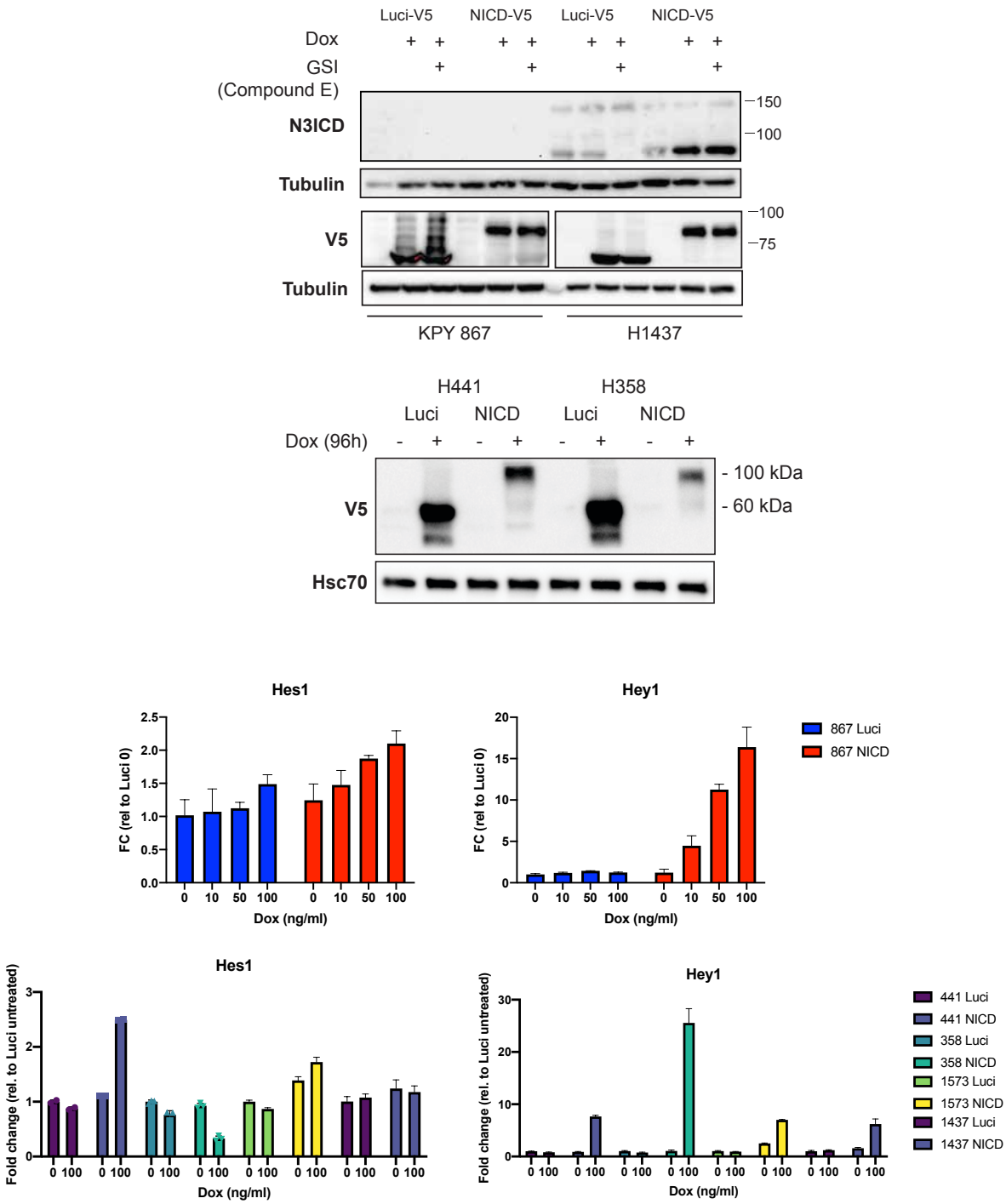

Figure 3.4 Expression and localization of NICD-V5 in lung adenocarcinoma cell lines. A) Western blots of cell lines expressing Luci-V5 and NICD3-V5. B) qPCR of Notch target expression after NICD induction with doxycycline in a dose-dependent (top, 72h) and cell line-dependent (bottom, 48 h) manner.

which is a best characterized as a downstream target of Notch1, which was only upregulated in the H441 cell line. Notably, H441 expresses a greater quantity of Notch1 (a known regulator of Hes1) relative to the other LUAD cell lines. Immunofluorescence imaging of the V5 epitope in naïve and dox-induced H358 cell lines indicated a diffuse, cytoplasmic distribution of the expressed construct in the luciferase cell line and exclusively nuclear distribution in the NICD cell line, suggesting appropriate localization of the construct (**Figure 3.5**).

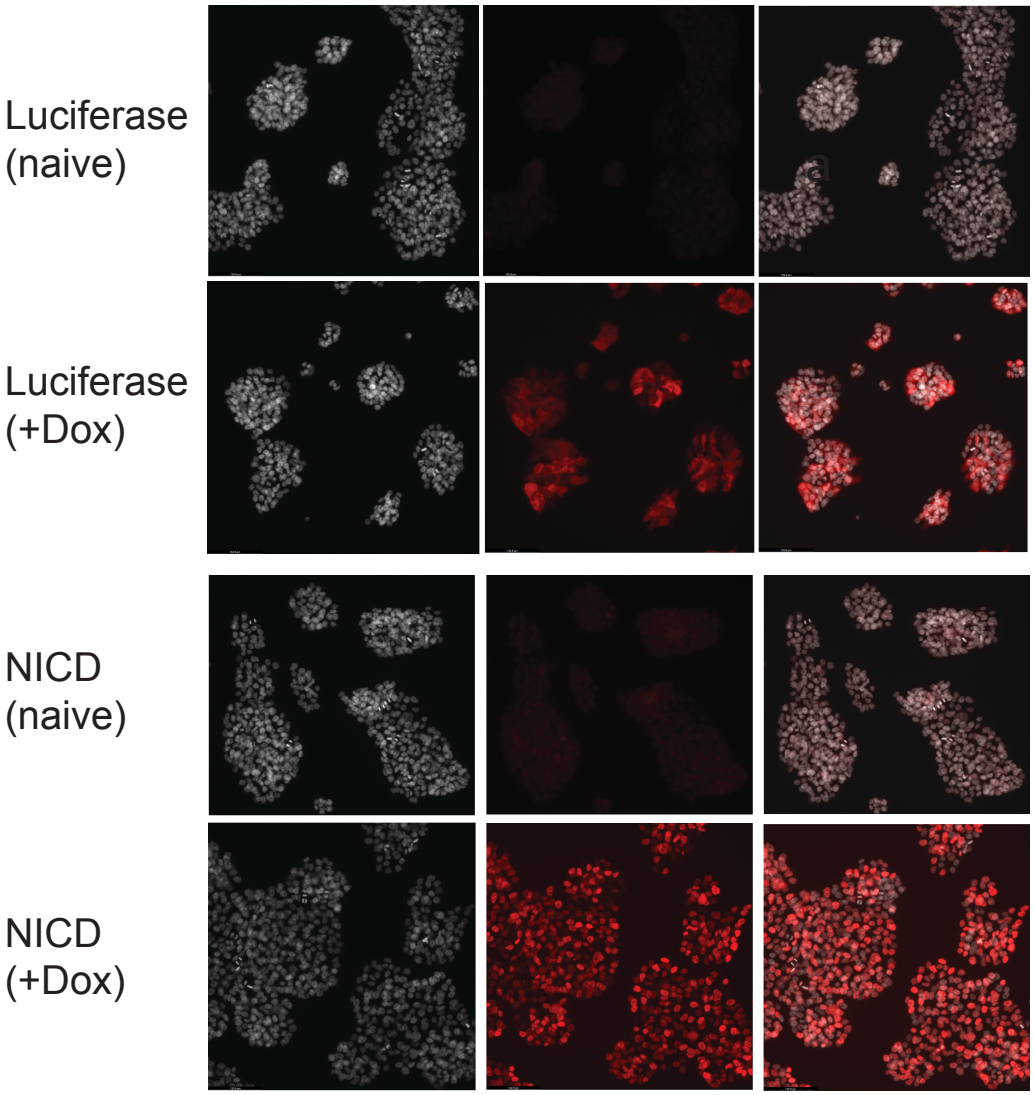

Figure 3.5 NICD-V5 expression localizes to the nucleus Immunofluorescence of H358 cell line for V5 expression (red) and DAPI (white) before (naïve) and after dox induction (20X objective, 800X total magnification).

Notch induction regulates cell morphologic, metabolic, and lineage-specific gene signatures

We performed transcriptomic analyses at 96 h post dox-induction from KPY867, H358, and H441 luciferase and NICD3-expressing cell lines. We used unsupervised principal component analysis of the KPY867 and human cell line data to confirm that the naïve (no dox) and luciferase with dox controls clustered together, in comparison to the Notch induced samples (**Figure 3.6 A-B**).

In our initial analysis, we hypothesized that Notch3 might regulate a common set of genes between the mouse and human cell lines; however, downstream analysis of the differentially expressed genes (DEGs) in the Notch induced condition revealed limited overlap: Only 13 DEGs were shared between all three cell lines, with minimal overlap between the human and mouse cell lines (**Figure 3.6 F**). Between the two human LUAD cell lines, we found 157 upregulated and 296 downregulated shared consensus genes which constituted 27% and 32% of all differentially expressed genes. Given a log-fold change and p-value thresholds of 1.2 and 0.01, respectively, only 17 genes were differentially regulated (i.e. upregulated in one cell line while downregulated in the other, or vice versa) between the two cell lines, including one Notch family member (Lunatic Fringe, LFNG) and WNT9A.

We also performed gene-set enrichment analysis (GSEA) for each cell line to identify any common pathways enriched after NICD3 expression (**Figure 3.6 C-E**, only KEGG shown). Broadly, we found altered regulation of extracellular matrix (ECM)/cell morphology and RNA/protein metabolic signatures. However, while a few pathways were shared (TGF-B signaling, Cytokine interactions positively enriched in KPY867 and H441; Axon guidance, ECM receptor interactions positively enriched in KPY867 and H358), no top pathways were positively

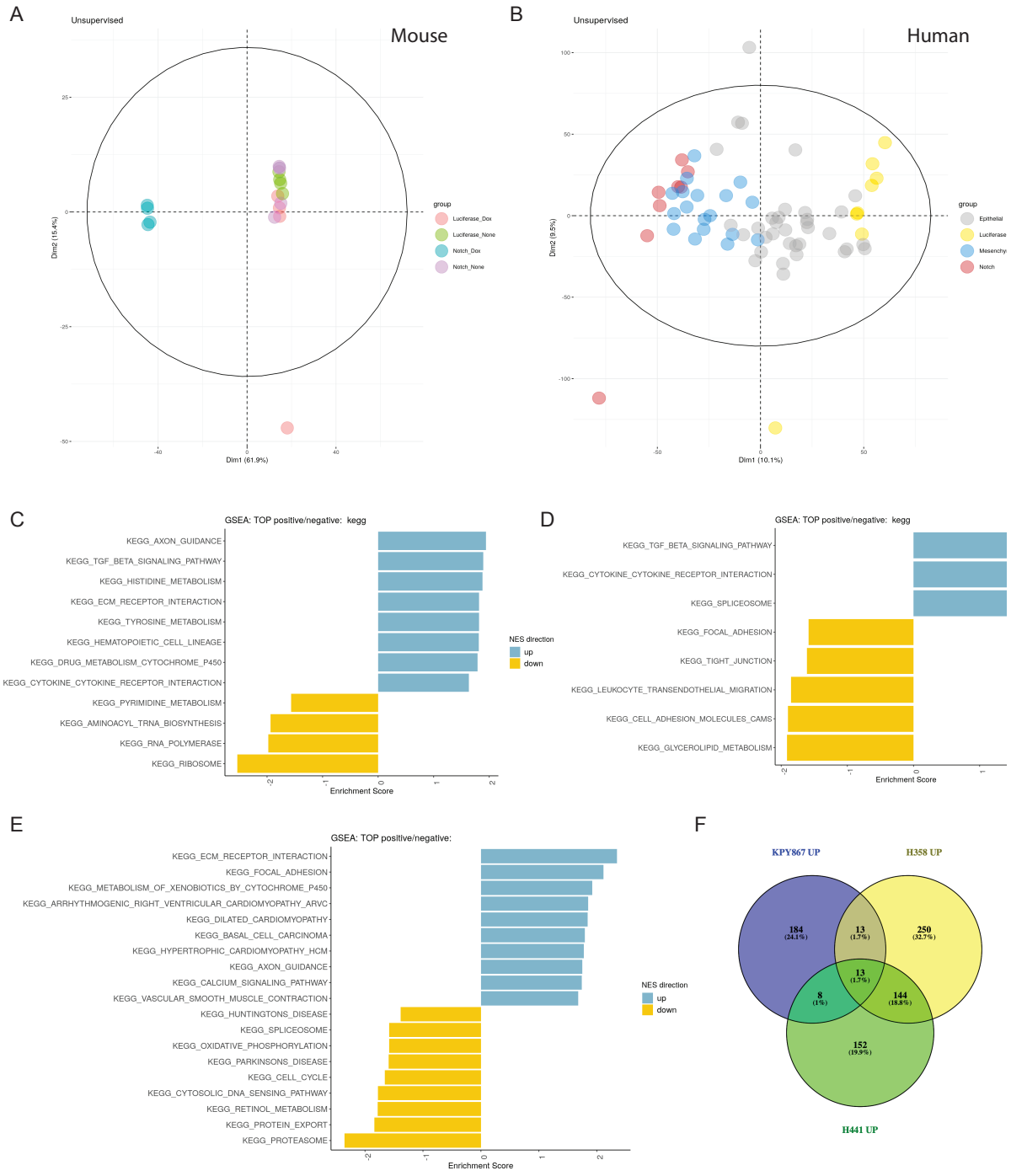

Figure 3.6 Gene expression analysis of NICD3-expressing cell lines 96 h post-induction. **A** Unsupervised principal component analysis (PCA) of KPY867 cell lines before and after dox induction. **B** Unsupervised PCA of CCLE LUAD cell lines alongside H358 and H441 luciferase (yellow) and NICD-induced (red) cell lines. CCLE LUAD cell lines (including parental H358 and H441) categorized as "epithelial" (grey) and "mesenchymal" (blue), with a threshold of E-cadherin:Vimentin log-fold change ratio > 2 for epithelial cell lines and <= 2 for mesenchymal cell lines. **C-E** GSEA KEGG pathway enrichment plots of NICD3-enriched gene sets for KPY867 (**C**), H441 (**D**), and H358 (**E**). **F** Venn diagram of up-regulated genes shared between the three NICD3-induced cell lines (LFC >= 1.2 and p-value < 0.01).

or negatively enriched in H441 NICD while the focal adhesion pathway was positively enriched in H358 NICD.

We hypothesized that cell-type specific differences in gene expression might account for the lack of overlap in pathways after gene set enrichment analysis. Thus, to discover Notch-dependent pathways common to both human cell lines while accounting for cell type-specific effects, we turned to Gene Set Variation Analysis (GSVA)[15]. This method utilizes an unsupervised approach to calculate pathway enrichment scores on a per-sample basis and then uses a rank statistic to determine whether the scores significantly differ between two groups of interest: in sum, the comparison of pathway scores rather than individual genes allows for a more robust, functional analyses within a heterogeneous population, e.g. cell lines with differences in baseline gene expression. We separated the GSVA analyses by pathway categories, which included KEGG, Hallmark and Reactome gene sets. These revealed largely overlapping signatures of strong downregulation of tight junction and focal adhesion gene sets, with a particularly strong negative enrichment of Rho and Rab GTPases among the Reactome gene sets (**Figure 3.7-9**). We also noted repeated downregulation of apoptosis genes alongside upregulation of DNA repair and cell cycle checkpoint genes, which might predict a chemoresistance and cell growth phenotype (**Figure 3.7**). However, there was simultaneously a downregulation of spindle checkpoint factors; this, coupled with mixed effects on cell cycle gene sets overall (**Figure 3.6 E, 3.7**), indicating that, in line with our *in vitro* cell growth data, NICD does not necessarily promote cell cycle progression but rather is more likely to modulate checkpoint blockade.

Another category of interest was metabolism: while many metabolic gene sets were downregulated, particularly those related to phospholipid signaling (**Figure 3.7-8**), oxidative

phosphorylation and Complex I were found among the few upregulated gene sets. In addition, we found upregulation of the mTORC1 gene set (**Figure 3.8**) as well as bidirectional regulation of PI3K-AKT signaling gene sets, the latter a likely consequence of downregulated phosphatidylinositol gene sets. Perhaps counterintuitively, we observed a consistent trend in downregulation of growth factor-dependent pathways, including ERBB, EGFR, and MET (**Figure 3.7, 3.9)** with mixed effects on KRAS signaling (**Figure 3.8**), suggesting a decreased reliance on signaling through these mechanisms. Together, these paint a picture of Notch-dependent metabolic alterations in the LUAD cell lines.

Finally, we made the observation that the KEGG "Non-Small Cell Lung Cancer" gene set itself was negatively enriched in NICD cell lines (**Figure 3.7**). We hypothesized that, despite the absence of canonical "stem cell" gene sets in our analyses, NICD may be promoting a state change in the LUAD cell lines towards a less-differentiated cell type relative to its parental lines, a feature that has long been linked with stemness-promoting factors[16,17]. We therefore extracted lineage markers used to identify non-immune human lung cell types in single-cell data[18] and examined their expression in our data set (**Figure 3.10 A**). Strikingly, around two-thirds of lineage-specific genes were downregulated with NICD3 expression, and unsupervised hierarchical clustering indicated that NICD expression drove greater similarity between samples than did parental cell type. When we examined specific gene signatures, we found that that expression of AT2-specific genes was primarily determined by the parental cell line, while AT1 and mucous-specific genes were determined by NICD expression, and that this was reinforced by the sample clustering patterns (**Figure 3.10 B-D**). Interestingly, a number of mucous-specific genes appeared to be upregulated, in contrast to AT1-type genes which were largely repressed. We noted that several of the AT1 lineage-specific genes, such as ANKRD1 and AXL, were well-

established targets of YAP1/TAZ, the major downstream effectors of the Hippo tumor suppressor pathway. We therefore examined the expression changes of a YAP/TAZ transcriptional signature[19], selected on the basis of its clinical prognostic power across multiple cancer types, of which 11 (out of 22 total) were expressed the H358 and H441 cell lines (**Figure 3.10 E**). Again we found common regulation between the two cell lines of both up- and downregulated genes in a NICD-dependent manner. This data supports the hypothesis that NICD expression modulates the expression of lung fate-specifying genes including YAP1/TEAD targets, particularly of but not exclusive to the mucous lineage state.

Notch3 transcriptional regulation occurs through both direct and indirect epigenetic targeting

While RNA-sequencing is a powerful technique for analyzing downstream expression, the discovery of genes directly regulated by a transcription factor is confounded by secondary feedback and in this case, non-endogenous expression. Since the Notch Transcriptional Complex (NTC) may modulate gene expression through both enhancer and promoter binding, we chose to use a proximity-based analysis as a common approach for assigning transcription factor binding sites to their most likely gene target[20].

In order to discover novel NICD3-bound sites, we utilized a protocol for native chromatin isolation called "Cut&Run" recently developed by the Henikoff lab[21,22]. In this protocol, unfixed cell lines are permeabilized, incubated with primary antibody, washed, and re-incubated with a protein A/G-conjugated MNase (**Supp. Figure 3.1 A**). Upon activation with calcium, pAG-MNase digests chromatin adjacent to the bound primary antibody, releasing chromatin-bound complexes from which DNA is extracted, amplified, and sequenced using short-read (PE25) format. Cut&Run provides a number of advantages over fixed chromatin immunoprecipitation,

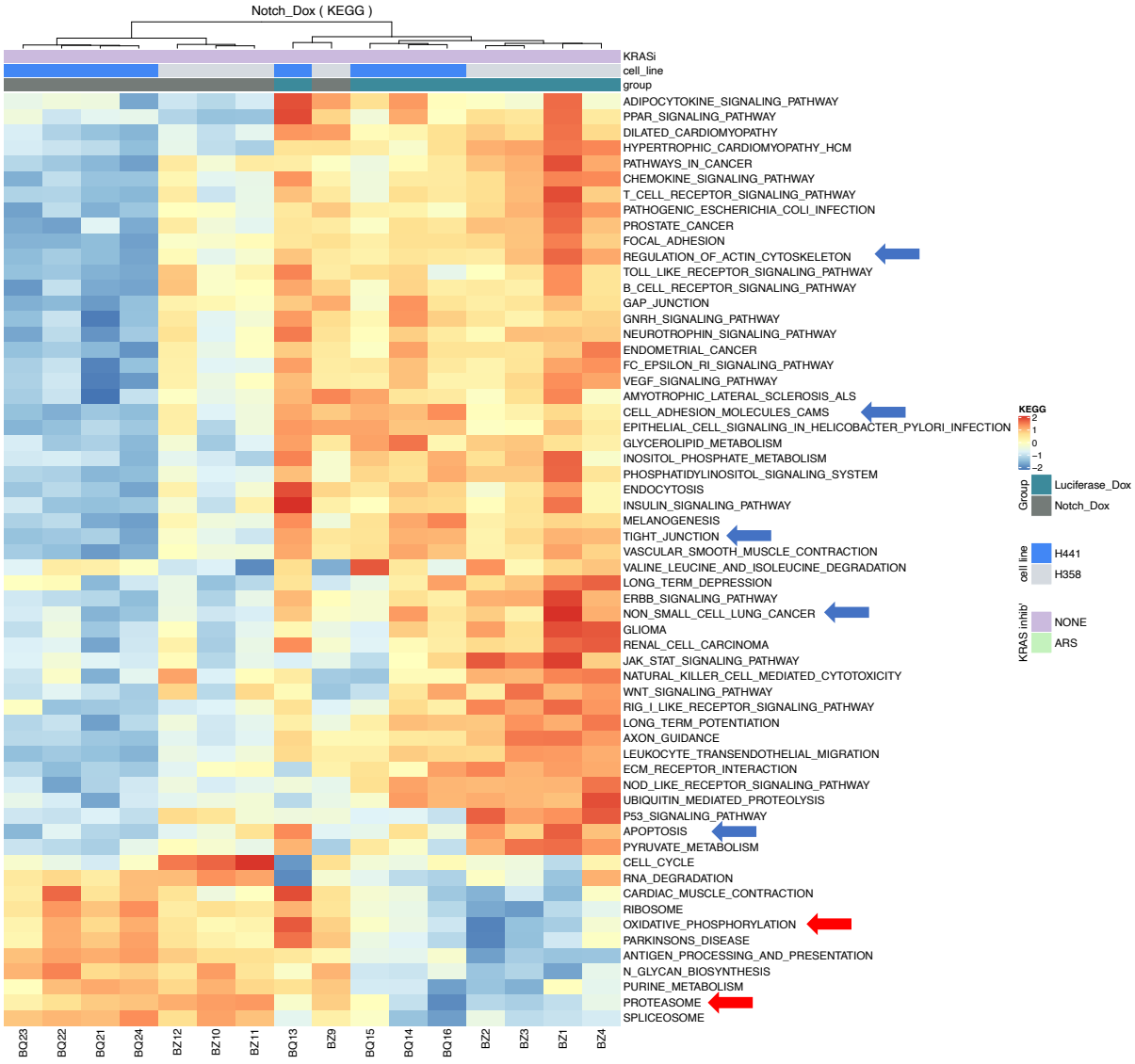

Figure 3.7 GSVA KEGG pathway enrichment of human Notch cell lines KEGG pathways enriched in H441 and H358 Notch Dox vs Luciferase Dox. Blue arrows indicate downregulated and red arrows indicate upregulated NICD pathways, respectively. Pathway enrichments ordered by lowest p-value.

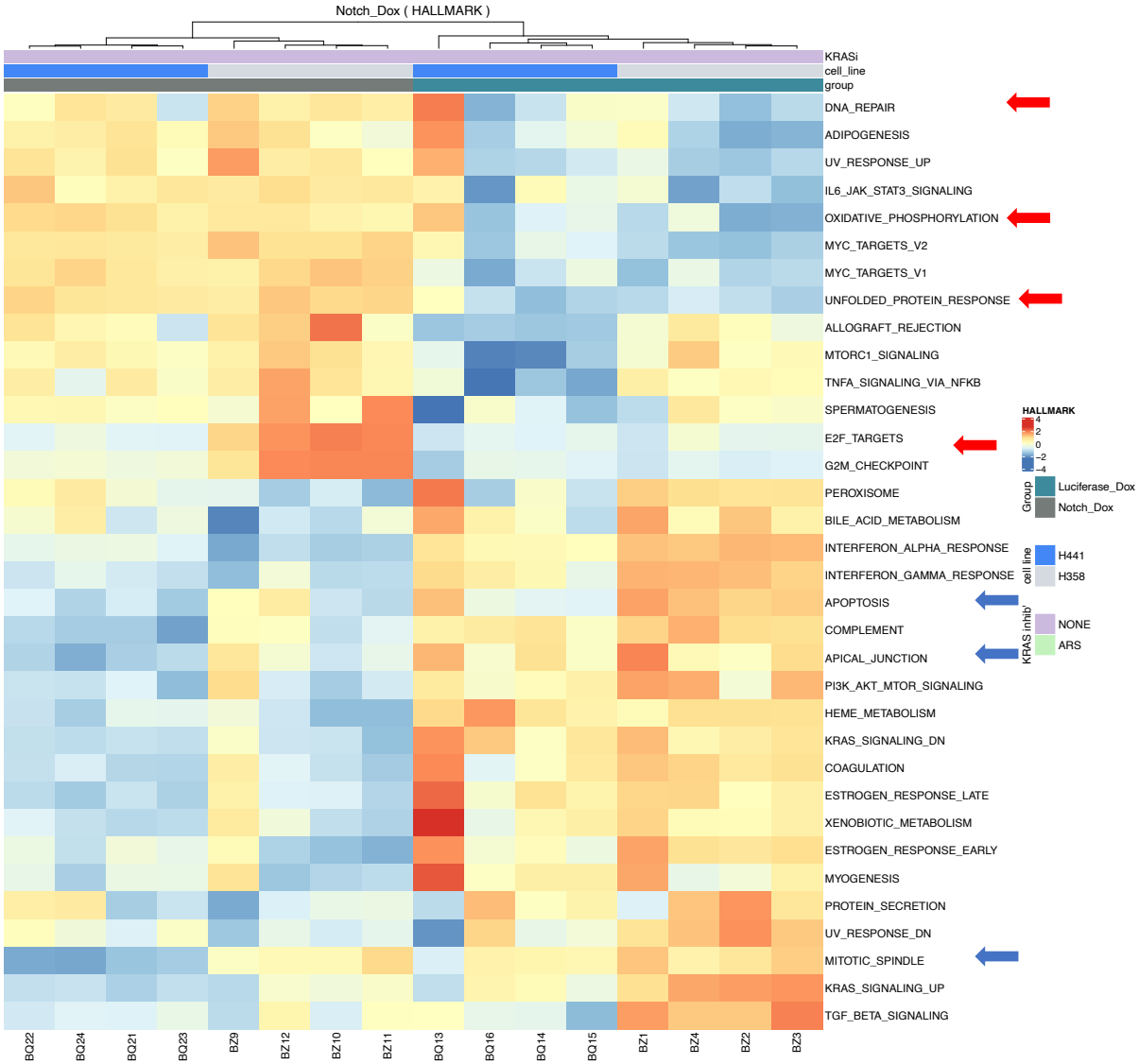

Figure 3.8 GSVA Hallmark pathway enrichment of human Notch cell lines. Hallmark gene sets enriched in H441 and H358 Notch Dox vs Luciferase Dox. Blue arrows indicate downregulated and red arrows indicate upregulated NICD pathways, respectively. Pathway enrichments ordered by lowest p-value.

Figure 3.9 GSVA Reactome pathway analysis of human Notch cell lines. Reactome gene sets enriched in H441 and H358 Notch Dox vs Luciferase Dox. Blue arrows indicate downregulated and red arrows indicate upregulated NICD pathways, respectively. Pathway enrichments ordered by lowest p-value.

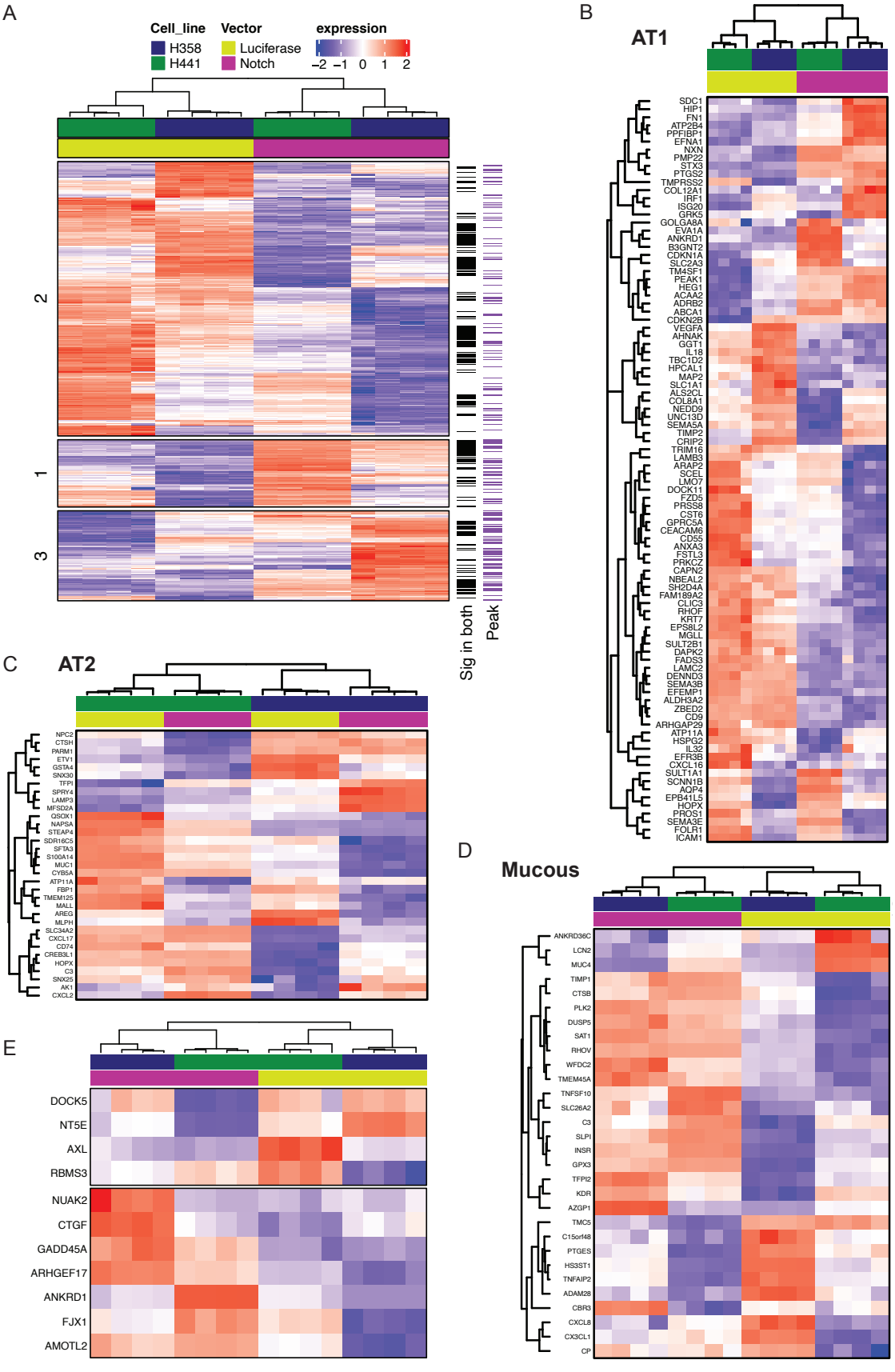
A
Cell_line
H358
H441
Vector
Luciferase
Notch
expression
−2 −1 0 1 2
2
1
3
Sig in both
Peak
B
AT1
SDC1
HIP1
FN1
ATP2B4
PPFIBP1
EFNA1
NXN
PMP22
STX3
PTGS2
TMPRSS2
COL12A1
IRF1
ISG20
GRK5
GOLGA8A
EVA1A
ANKRD1
B3GNT2
CDKN1A
SLC2A3
TM4SF1
PEAK1
HEG1
ACAA2
ADRB2
ABCA1
CDKN2B
VEGFA
AHNAK
GGT1
IL18
TBC1D2
HPCAL1
MAP2
SLC1A1
ALS2CL
COL8A1
NEDD9
UNC13D
SEMA5A
TIMP2
CRIP2
TRIM16
LAMB3
ARAP2
SCEL
LMO7
DOCK11
FZD5
PRSS8
CST6
GPRC5A
CEACAM6
CD55
ANXA3
FSTL3
PRKCZ
CAPN2
NBEAL2
SH2D4A
FAM189A2
CLIC3
RHOF
KRT7
EPS8L2
MGLL
SULT2B1
DAPK2
FADS3
LAMC2
DENND3
SEMA3B
EFEMP1
ALDH3A2
ZBED2
CD9
ARHGAP29
ATP11A
HSPG2
IL32
EFR3B
CXCL16
SULT1A1
SCNN1B
AQP4
EPB41L5
HOPX
PROS1
SEMA3E
FOLR1
ICAM1
C
AT2
NPC2
CTSH
PARM1
ETV1
GSTA4
SNX30
TFPI
SPRY4
LAMP3
MFSD2A
QSOX1
NAPSA
STEAP4
SDR16C5
SFTA3
S100A14
MUC1
CYB5A
ATP11A
FBP1
TMEM125
MALL
AREG
MLPH
SLC34A2
CXCL17
CD74
CREB3L1
HOPX
C3
SNX25
AK1
CXCL2
D
Mucous
ANKRD36C
LCN2
MUC4
TIMP1
CTSB
PLK2
DUSP5
SAT1
RHOV
WFDC2
TMEM45A
TNFSF10
SLC26A2
C3
SLPI
INSR
GPX3
TFPI2
KDR
AZGP1
TMC5
C15orf48
PTGES
HS3ST1
TNFAIP2
ADAM28
CBR3
CXCL8
CX3CL1
CP
E
DOCK5
NT5E
AXL
RBMS3
NUAK2
CTGF
GADD45A
ARHGEF17
ANKRD1
FJX1
AMOTL2

methods, as it avoids sonication/fixation artifacts, requires lower sequencing depth, and allows for greater multiplexing capacity. Its disadvantages include the limited number of validated antibodies and challenging troubleshooting, as low chromatin output prohibits the use of qPCR to amplify post-Cut&Run DNA, generally requiring sequencing to determine whether a reaction was successful.

We developed a pipeline for processing the Cut&Run data using a previous pipeline, Cut&Run Tools[23], as a model, with additional integration of spike-in calibrations and DESeq2 comparisons between samples (**Supp. Figure 3.1 A-B**). We performed and fully analyzed Cut&Run for V5, IgG control, and K27Ac histone marks in the H358 NICD3 condition after 96 h of dox induction. While we also performed preliminary analysis of H441 NICD3 cell line, we were able to detect very few V5 peaks possibly due to the low signal-noise ratio (**Supp. Figure 3.1 C**) and thus primarily focused our genome-wide analysis efforts on the H358 cell line.

Taking all 5600 high-confidence V5 peaks, we first asked whether we could enrich for Rbpj motif binding, as would be expected for the canonical Notch Transcriptional Complex (NTC). We used MEME (Multiple Em Motif Enrichment)[24] as an unbiased method to search for universally enriched sequences between 7-21 bp long (default MEME setting) within the annotated peak regions. Of the three reported motifs, the only non-degenerate sequence found was a complete match for the JASPAR Rbpj motif, with a slight preference for two cytosine residues immediately upstream of the motif sequence. This *de novo* analysis confirmed that our expressed Notch-ICD indeed bound Rbpj motifs as previously observed (**Supp. Figure 3.2**).

Figure 3.10 RNA-seq expression heatmaps of lung cell lineage-specific genes. A All expressed lineage-specific genes, black denotes LFC magnitude > 1.2 and p-value < 0.01, purple denotes presence of V5 peak from Cut&Run data in H358. **B** AT1-specific genes. **C** AT2-specific genes. **D** Mucous-specific genes. **E** YAP/TAZ signature genes.

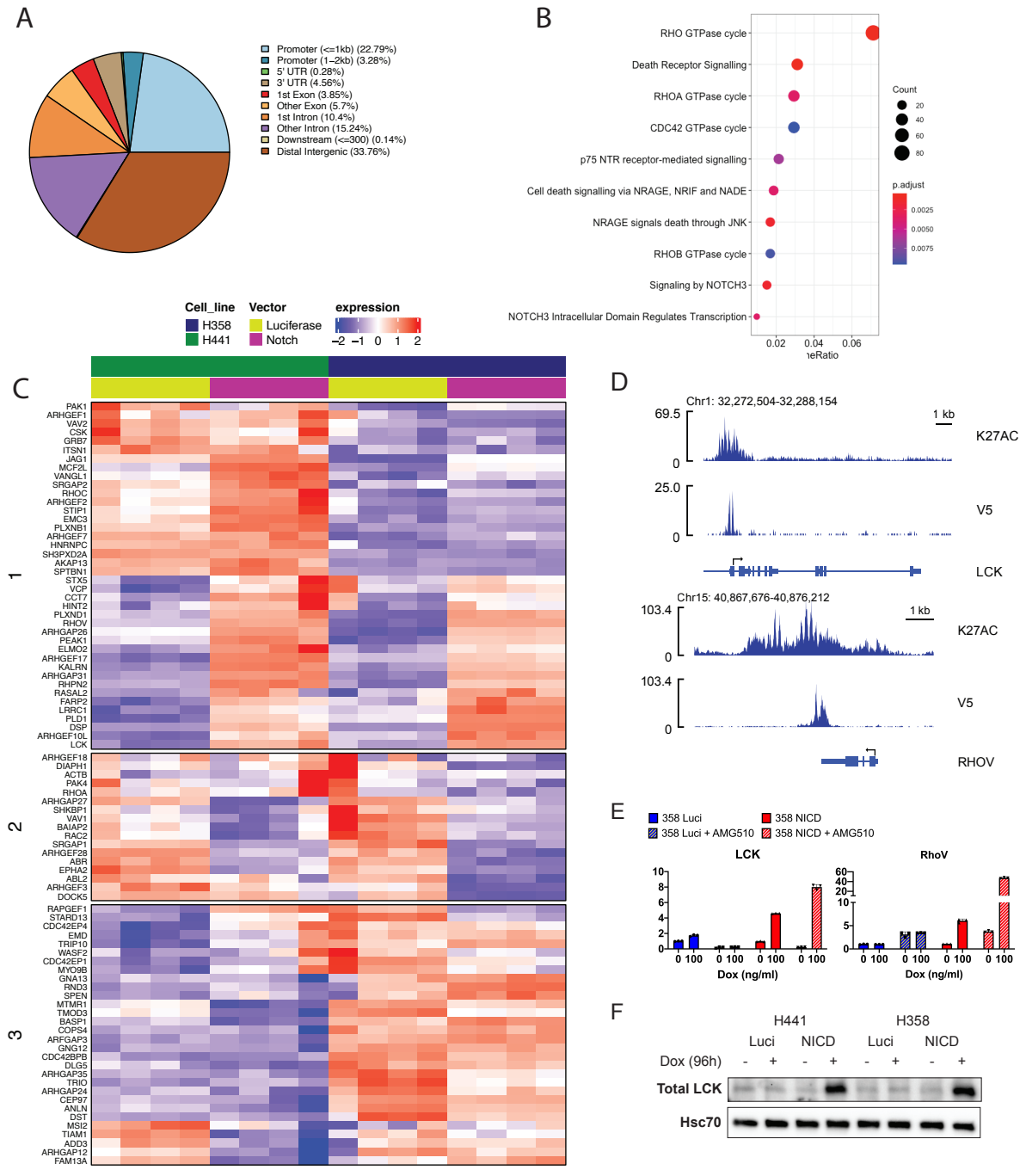

Figure 3.11 NICD3 epigenomic activity modulates expression of Rho family genes. A Distribution of all V5 peaks among known genomic features. **B** Over-representation analysis of Reactome pathways enriched in NICD-bound genes. **C** Gene expression heatmap of all NICD-bound Rho pathway genes (as defined by gene sets in B). **D** Cut&Run NICD-V5 and K27Ac tracks of Lck and RhoV in H358 NICD cell lines. **E** Expression of RhoV and Lck in H358 luciferase and NICD cell lines, with or without sotorasib (AMG-510) treatment (4 h, 1 μM) after doxycycline induction (48 h). **F** Western of total Lck protein across LUAD luciferase and NICD cell lines.

We next analyzed the genome-wide distribution of H358 V5 peaks and confirmed these were predominantly located within 2 kb of annotated promoters or within gene bodies (**Figure 3.11 A**). Interestingly, of the 665 V5 annotated peaks, only 161 were assigned to genes which were differentially regulated in the RNA-seq data. Of these, a disproportionate number were upregulated: 27.8% of upregulated genes were annotated with V5 peaks (117/420), while only 6.7% of downregulated genes were annotated (44/657). We infer this to suggest NICD-downregulated genes are primarily regulated through indirect regulation, i.e. by upregulation of transcriptional repressors such as Hes/Hey family members, rather than direct repression at the promoter itself, whereas NICD upregulated genes are more likely to be regulated through promoter binding in a direct regulatory manner. Notably, this analysis was limited to promoter-bound peaks, and thus is unable to assess whether NICD might act in an activating or repressive capacity at enhancers. These findings contrast with other cell line epigenomic data, most notably in T-ALL, where Notch appears to act largely through distal super-enhancer regions[25]. However, these findings are not incompatible with Notch3 acting as a distal enhancer, as two-dimensional distance alone is not predictive of a transcriptional target; rather, three-dimensional conformational data and is required to determine what gene "neighborhoods" are most likely regulated by a given regulatory peak[26]. Given such models, we would predict that NICD likely activates a subset of non-annotated upregulated genes through enhancer interactions.

We then searched for common gene sets and found strong enrichment of Rho family-related pathways, including the Rho GTPase cycle and G alpha (12/13) signaling events (**Figure 3.11 B**). Other pathways included cell junction organization, death receptor/JNK signaling, TGF-B signaling, and Notch signaling. Perhaps counterintuitively, the most strongly enriched pathway (Rho GTPase cycle) was downregulated in the GSVA Reactome analysis across the two NICD

cell lines; however, closer examination of the V5-marked genes revealed that the Rho pathway broadly clustered into three categories: **1** upregulated, **2** downregulated, and **3** cell line-dependent (**Figure 3.11 C**). Examining individual peak regions, we found that most V5 peaks were distributed throughout the gene body, both upstream and downstream of promoters, and often associated with a subtle decrease in the K27Ac peak (**Figure 3.11 D**).

Several of the Rho family V5-marked genes, including Lck and RhoV, were strikingly upregulated by NICD in both cell lines. Both Lck and RhoV have been previously implicated in the regulation of a key Rho GTPase effector kinase, PAK1, whose promoter also harbors a NICD peak in the Cut&Run analysis (**Supp. Figure 3.3**) suggesting that NICD may act as a transcriptional regulator of a Lck/RhoV-PAK1 module. We validated the upregulation of both Lck and RhoV in H358 NICD cells by qPCR (**Figure 3.11 E**) as well as Lck protein expression in both cell lines (**Figure 3.11 F**). Given that the tyrosine kinase Lck was previously implicated as uniquely activated in a Kras-dependent manner in LUAD cell lines[27], we asked whether NICD-mediated regulation of Lck was also Kras-dependent and assessed both Lck and RhoV expression after Kras inhibition. Unexpectedly, we found that Lck and RhoV expression drastically increased upon Kras inhibition in the setting of Notch activation, suggesting that Kras activity antagonizes NICD modulation of Rho signaling.

NICD3 expression induces an epithelial-to-mesenchymal state change in LUAD

Given our initial observation of the phenotypic changes occurring with NICD expression in Kras mutant LUAD cell lines, coupled with NICD-dependent transcriptional regulation of genes related to cell morphology and attachment, we investigated whether NICD expression might promote the mesenchymal state in epithelial LUAD cell lines. After 96 h of induction, we

detected increased protein abundance of master EMT (epithelial-to-mesenchymal) regulators Snail and Slug in H358 and H441 NICD cell lines, but no change in overall E-cadherin levels (**Figure 3.12 A**). N-cadherin, a cell adhesion transmembrane protein typically associated with mesenchymal cells, increased in the H358 cell line but remained undetectable in H441. After carrying dox induction out to day 10, we found downregulation of E-cadherin in H441 which coincided with strong upregulation of EMT regulator Zeb1 (**Figure 3.12 C**) not seen in H358.

Immunofluorescence of H441 luciferase and NICD cells from this timepoint revealed an increase in nuclear Slug staining in the NICD cells, as well as loss of E-cadherin signal at cell borders with retention of nuclear staining, suggesting the intracellularization of E-cadherin (**Figure 3.12 B**). We also assessed the transcript expression of Snail and Has2, previously reported as an EMT master regulator downstream of Kras/TGFβ-mediated EMT in PDAC[28]. Has2 was upregulated in all except for Kras-wildtype H1437, while Snail was upregulated in all but H441, possibly due to negative feedback from pre-existing Snail expression at baseline (**Figure 3.12 D**). Finally, we assessed the protein expression of tight junction proteins and observed strong Zo-2, Zo-3 and claudin downregulation in a Notch-dependent manner (**Figure 3.12 C**). Zo-1 remained unaffected, consistent with previous reports of Snail-mediated downregulation of tight junction proteins[29].

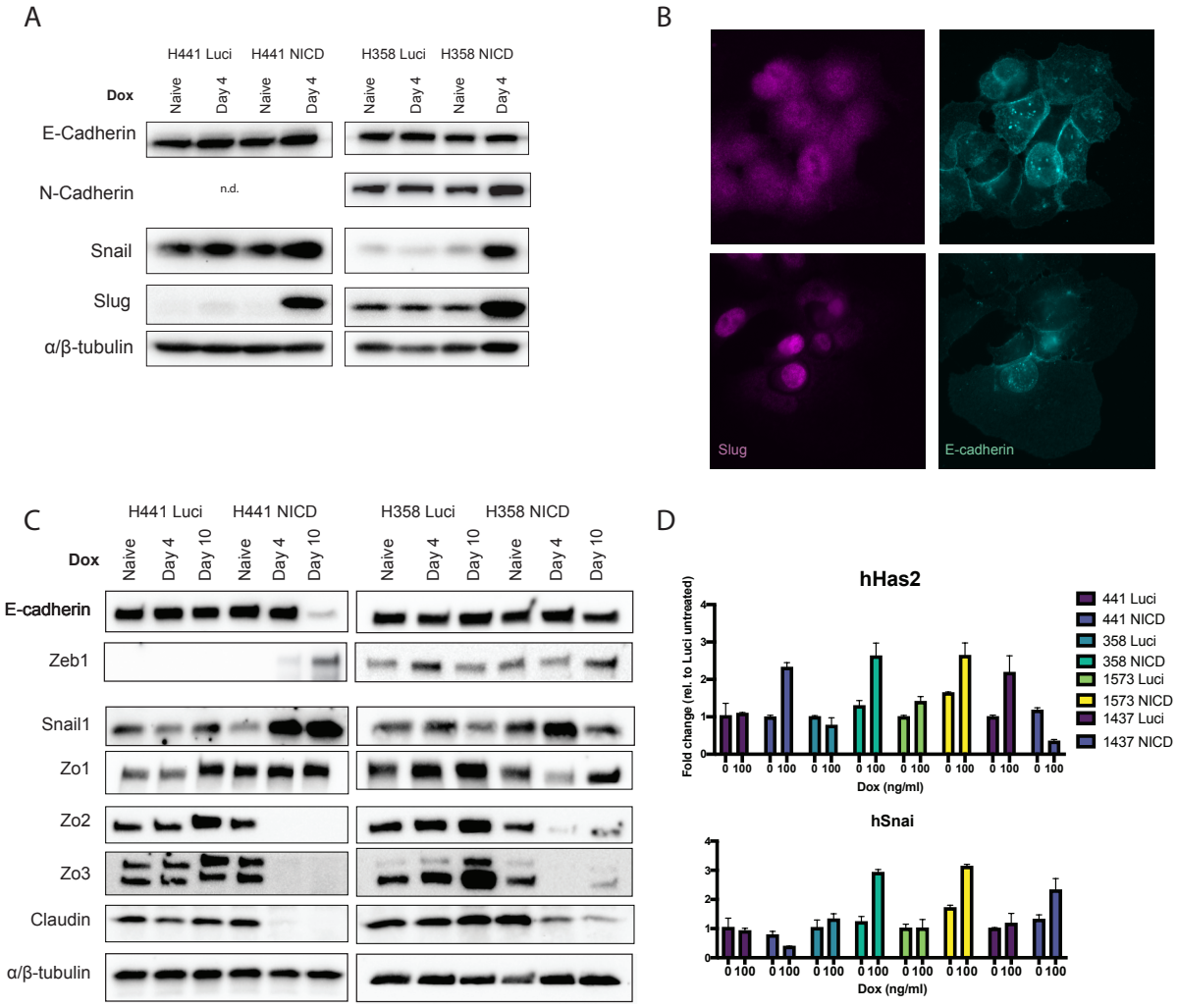

Figure 3.12 NICD3 induces pro-mesenchymal state in epithelial LUAD cell lines. A WB of cell adhesion-regulating cadherins and EMT transcription factors after 4 d. **B** Immunofluorescence of Slug and E-cadherin in H441 luciferase (top panels) and NICD (bottom) after 4 d. **C** WB of EMT and tight junction proteins after an extended time course of NICD induction. **D** qPCR of Has2 and Snail expression after 72 h of dox induction in 4 LUAD cell lines. All cell lines harbor at least one Kras mutant allele except for H1437.

Examination of the Cut&Run data from the H358 cell line revealed a weak peak in the Slug promoter region (**Supp. Figure 3.3**) and no peak proximal to Snail, indicating that robust upregulation of these two genes is likely not due to NICD directly. We also observed no enrichment of EMT-specific signatures in the earlier gene set analyses, suggesting that NICD expression may promote an incomplete state transition. In support of this, we found no evidence of increased migratory or invasive capacity in the NICD cell lines using standard Boyden chamber or scratch assays (data not shown). Though these were hindered by the negative effect of NICD expression on cell growth (**Supp. Figure 3.4 A**), we found that H358 cell lines implanted subcutaneously *in vivo* clearly demonstrated dox-induced tumor growth with NICD but not luciferase expression (**Figure 3.13**). We found similar growth effects in pilot studies of H441 and H1573 NICD cell lines (**Supp. Figure 3.4 B**).

Given these observations, we postulate that, in addition to acting as a transcriptional activator, NICD may function to repress tumor suppressors such as the FoxO family members. FoxO1, for example, is a well-known repressor of Snail and Slug, and Notch-mediated upregulation of AKT/mTor signaling may be sufficient to suppress nuclear FoxO1 activity. This type of activity is also consistent with NICD modulation of the Hippo tumor suppressor pathway genes observed earlier (**Figure 3.10 E**), and could potentially explain the rapid NICD-driven growth *in vivo* in the absence of any such effect *in vitro*.

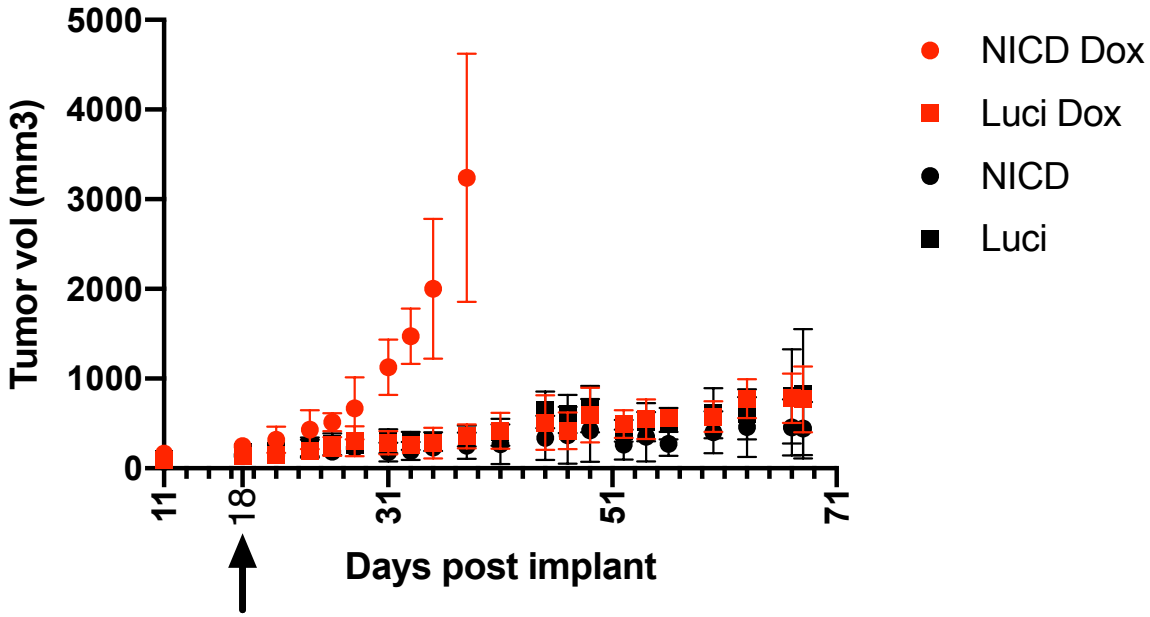

Figure 3.13 NICD3 induction increases tumor growth rate in the H358 xenograft model. NSG mice subcutaneously implanted with $1x10^6$ cells/flank of naive H358 luciferase or NICD3 cells and administered doxycycline chow after tumors reached an average of 100 cm^3, measured three times weekly, and sacrificed upon reaching endpoint.

Notch-mediated EMT modulates resistance to small molecule KRAS(G12C) inhibition

The recent development of covalent KRAS(G12C) inhibitors has dramatically altered the treatment landscape of KRAS mutant tumors, particularly in lung adenocarcinoma where 85% of tumors are driven by KRAS mutations and nearly half (46%) occur as G12C missense substitutions[30]. Early clinical trial data from late-stage LUAD patients are extremely promising, though outcomes in other cancer types appear less clear-cut[31,32]. However, regardless of upfront sensitivity to targeted Kras inhibition, nearly all LUAD tumors will eventually stop responding to treatment and show disease progression[33]. Comprehensive molecular profiling of acquired resistance mutations revealed a number within RTK/RAS/MAPK/PI3K signaling pathways, including point mutations at the drug-binding pocket of KRAS and the appearance of non-G12C mutations in the other allele, indicating that many of these tumors (15/38) remain dependent upon RAS pathway activation. Intriguingly, KRAS(G12C) mutations were found at resistance in 15 of 17 patients, suggesting that the founder G12C-mutant clone acquired additional mutations upon expansion, rather than expansion of surviving passenger (non-G12C) clones after initial treatment[33]. Non-RTK related resistance mechanisms are also apparent: many relapsed tumors (11/38) harbored no identifiable mutations in aforementioned pathways, and two resistant tumors that contained no identifiable RAS mutations other than the original G12C mutation demonstrated histological transformation from adenocarcinoma to squamous-cell carcinoma, as has been previously observed in relapsed tumors after targeted EGFR therapies[34]. Therefore, it is of great interest to discover putative mechanisms that allow cells to bypass their RAS dependency either in an innate or acquired manner.

Several reports over the last two years have suggested that the acquisition of mesenchymal features (i.e. EMT) is a non-genetic resistance mechanism to covalent KRAS

inhibition as has been previously shown for other targeted therapies[11,14,35,36]. Given our identified role for Notch3 in tumor propagation in the GEMM context, alongside our cell line data supporting Notch3 as an EMT regulator in LUAD, we investigated whether Notch3 might thereby induce resistance to KRAS inhibition in our G12C-mutant H358 LUAD cell line.

To assess the effect of NICD3 on treatment response, we plated H358 luciferase and NICD3 cells either with or without doxycycline, added G12C inhibitor ARS-1620 the next day, and read out cell viability at five days post-drug using CellTiter Glo in 2D (**Figure 3.14 A**). We found that NICD3 cell lines had significantly increased resistance to treatment in a doxycycline-dependent manner. We also found similar results with sotorasib (AMG-510) in both 2D and 3D dox-treated cells (**Supp. Figure 3.5**), which as previously demonstrated, had a lower IC50 in our parental/control cell lines (~0.1 μM for sotorasib vs. 3.0 μM for ARS-1620 in 2D, 0.005 μM for sotorasib in 3D). We therefore chose to use sotorasib for most assays shown in **Figures 3.14 B-D** and in **Figure 3.16** unless noted otherwise.

Since the primary response to G12C inhibition is G1 arrest, followed by p21/p27 expression and cellular senescence[37], we treated dox- or naive cells with sotorasib for 24 h, labeled the cells with FITC-BrdU for 1 h, and used flow cytometry to analyze their respective cell cycle states (**Figure 3.14 B**). As expected, sotorasib treatment of Luciferase and NICD3-naive cells resulted in significant G1 arrest. Strikingly, significantly fewer Notch-dox treated cells appeared in G1 as cells continued to transit through S phase. Examination of the MAPK and PI3K/AKT signaling pathways downstream of RAS in NICD3-dox cells demonstrated a delayed loss of phospho-AKT, increased levels of total ERK and AKT, as well as delayed p21 upregulation (**Figure 3.14 C**). Interestingly, phospho-ERK was equivalently downregulated in

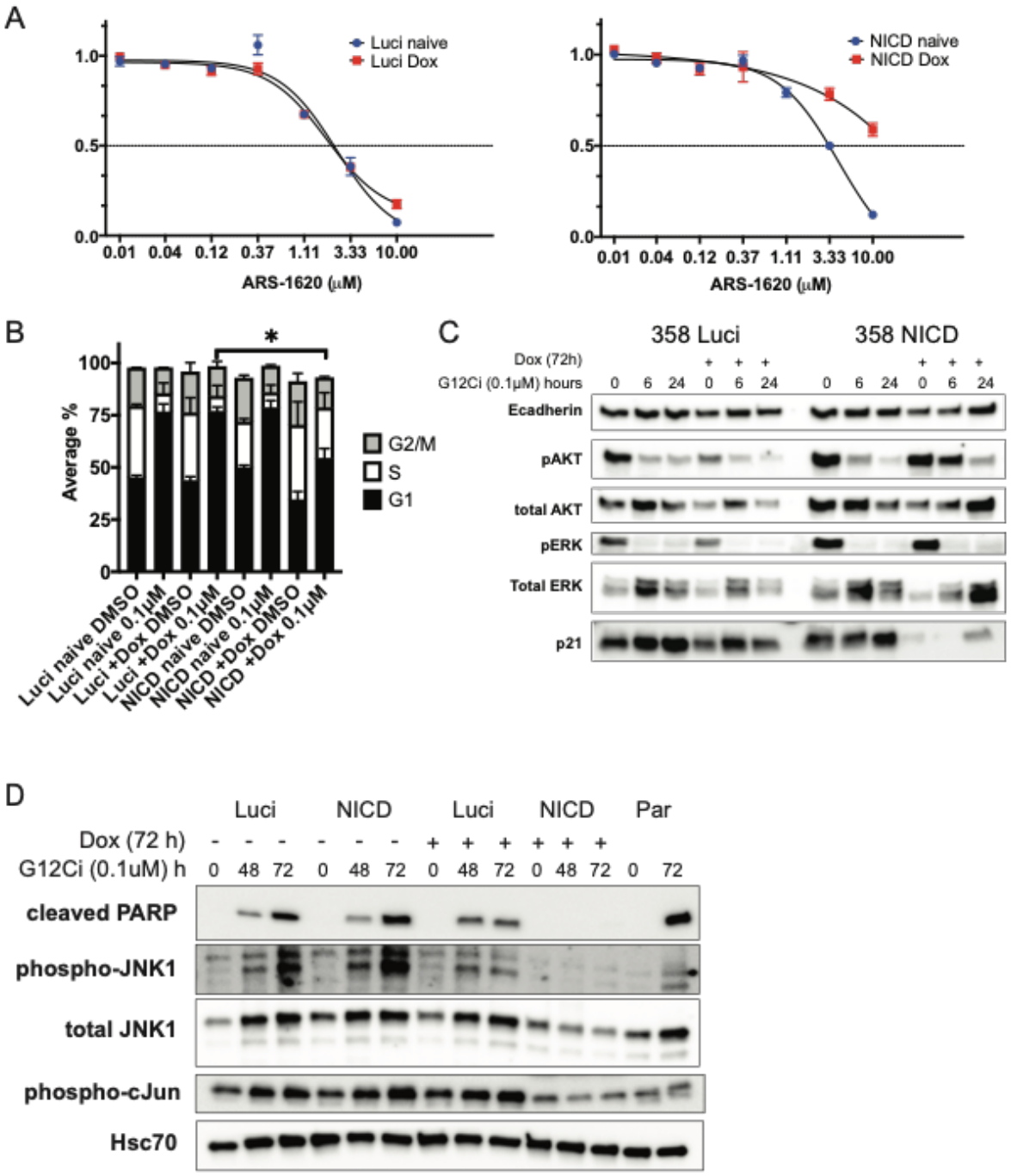

Figure 3.14 NICD3 induces resistance to KRAS(G12C) inhibitor *in vitro*. A 2D cell viability of luciferase (left) and NICD3 (right) cell lines in the presence (red) or absence (blue) of doxycycline after 5 days of treatment with ARS-1620. **B** Cell cycle progression following 24 h of treatment with sotorasib of either naive or pre-induced luciferase and NICD3 cell lines (3 d). **C** Western blot of RAS downstream signaling pathways at 6 h and 24 h after sotorasib treatment. **D** Western blot of apoptosis pathway markers after 48 h and 72 h in naive and pre-induced cell lines, and parental (Par) H358 cells.

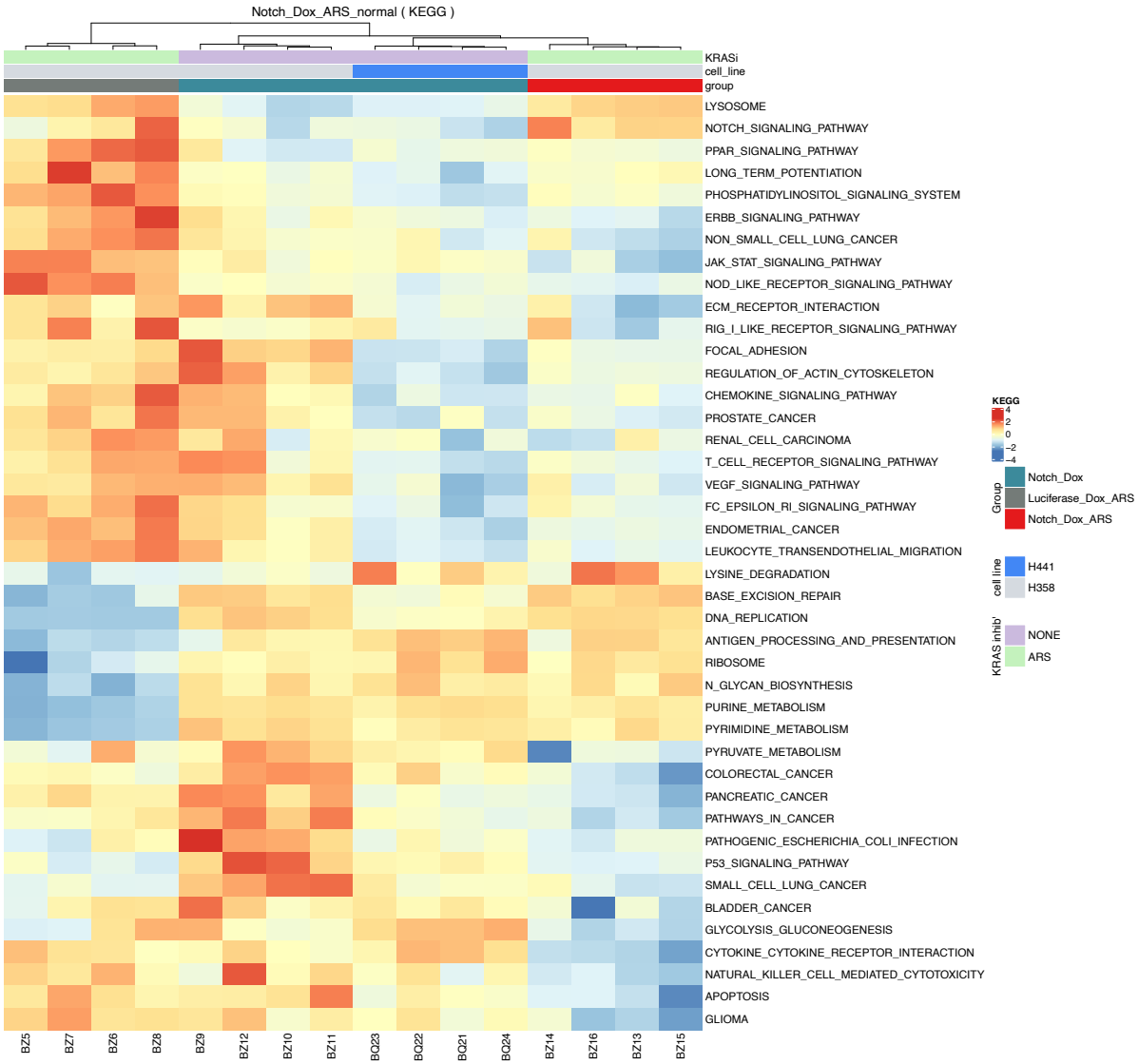

Figure 3.15 KEGG pathway enrichment analysis of H358 NICD3 with G12Ci. GSVA of KEGG pathways enriched in H358 Luciferase and NICD3-Dox cells with 24 h of ARS-1620 treatment, clustered relative to H358 NICD3-Dox and H441 NICD3-Dox untreated cell lines.

NICD3-dox and no dox conditions. This finding agreed with our previous RNA-seq findings that NICD3 primarily upregulates PI3K/AKT/mTor signaling rather than the MAPK pathway.

We then asked whether cell death pathways might be repressed in NICD3 sotorasib-treated cells in a dox-dependent manner (**Figure 3.14 D**). We found no detectable PARP cleavage up to 72 h after sotorasib treatment, as well as downregulation of JNK1/cJun, which are believed to act upstream of PARP cleavage in the coordination of intrinsic apoptosis[38]. From these data, we concluded that NICD3 expression is sufficient to induce cellular resistance to KRAS(G12C) inhibition.

We also performed RNA-sequencing on H358 luciferase and NICD3-dox induced cells after 24 h of treatment with either DMSO or 1.0 μM of ARS-1620. Strikingly, even though unsupervised principal component analysis indicated clustering of drug- with DMSO-treated cells (**Supp. Figure 3.7**) , GSVA of the most-differentially expressed pathways revealed that the ARS-1620 treated cells more closely resembled untreated NICD3-expressing H358 and H441 cell lines (**Figure 3.15**). In particular, we noted maintained upregulation of ribosomal and DNA repair/replication pathways in ARS-1620 NICD cells relative to Luciferase cells, consistent with their continued proliferation and escape of G12C inhibitor (G12Ci)-mediated G1 arrest. We also observed upregulation of antigen processing and presentation pathways that are downregulated in G12Ci-treated Luciferase cells, hinting that G12Ci-treated NICD cells may be able to evade immune surveillance more effectively than non-NICD G12Ci treated cells.

To discover Notch targets modulating G12Ci resistance in an unbiased manner, we performed a focused CRISPRi screen of Notch-upregulated genes and imputed co-transcriptional regulators in H358 dCas9 cells expressing either luciferase or NICD3 in an inducible manner. We passaged H358 dCas9 Luciferase-dox, NICD3-dox, and NICD-naive cells for up to 14 days

in culture with either DMSO or sotorasib, harvesting cells at matched timepoints, and analyzed the amplified sgRNA libraries for targets selectively depleted in sotorasib conditions. To account for viability phenotypes unrelated to sotorasib, we normalized the gene β-scores to their equivalent in DMSO control and plotted the resulting delta of β-scores, where a negative score indicates depletion in sotorasib relative to DMSO (**Figure 3.16 A**). As expected, we found more positive hits in the NICD3-dox condition since our screen design was limited to NICD3-upregulated targets. Reassuringly, our strongest positive controls (EGFR and CRKL) were strongly depleted in both the NICD3-dox and luciferase-dox sotorasib-treated conditions.

We immediately noticed that genes selectively depleted in NICD-dox + sotorasib were enriched in several categories, including EMT, Notch, and RAS pathways. Hey1, a strongly NICD3-dependent gene, was selectively depleted after sotorasib treatment in NICD3-dox but not Luci-dox cells, while Sox9 did not show any selective depletion due to its strong viability effect in NICD3-dox DMSO cells (**Supp. Figure 3.6 A**). Intriguingly, the positive control CDK4 scored strongly in Luci-dox cells as expected, but did not score in NICD3-dox cells. We confirmed that CDK4 was not a dependency in NICD-dox cells but confirmed it was moderately depleted in NICD-naive cells and strongly depleted in Luciferase-dox cells (**Supp. Figure 3.6 B**). CCND1 also did not score in NICD-dox and scored weakly in Luci-dox. Within the KRAS family, NICD-dox + sotorasib was more strongly depleted for GRB2 and slightly less dependent on KRAS than Luci-dox + sotorasib cells, suggesting that GRB2 or SHP2 inhibitors[39] may be effective against LUAD cells with a Notch3-high transcriptional program.

Strikingly, we observed a clustering of EMT family genes, including Snail (SNAI1), Slug (SNAI2), and CDX1 were strongly and selectively depleted in NICD3-dox cells + sotorasib. Notably, these genes have not scored in prior genome-wide CRISPR screens of sotorasib-

sensitizing genes, likely because the cell lines tested (including H358) were not in an EMT-state and consequently not expressing these targets. Thus, our data highlights the importance of using both sensitive and resistant models to discover the targets modulating drug sensitivity as these will likely depend upon the cell context. We also probed for Rho pathway regulator Lck and EMT protein expression after sotorasib treatment with or without dox induction, and we found that sotorasib treatment downregulated these factors, as well as upregulating ZO-3, with no effect on E-cadherin (**Figure 3.16 B**) We observed a similar trend for another Rho-related NICD3 target, Rock2, as well as vimentin (**Figure 3.16 C**). Notably, vimentin transcript was not present in our RNA-seq data for unknown reasons and therefore excluded from our screen; however, neither RhoV nor Lck scored as hits in our screen, suggesting that these may not be required for NICD3-induced sotorasib resistance.

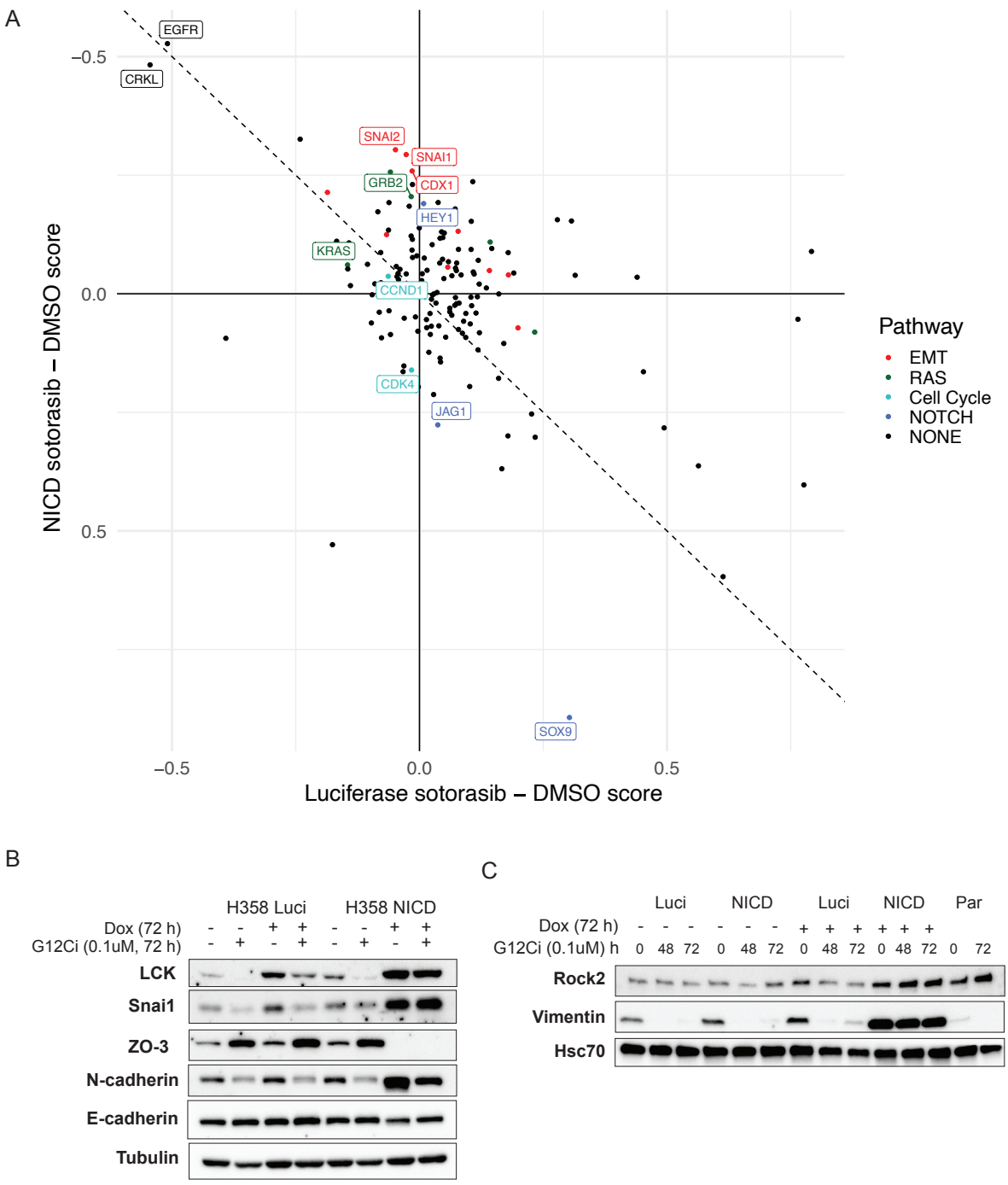

Figure 3.16 CRISPRi screen uncovers NICD3-selective dependencies in H358 cells. A Scatter plot of difference in sotorasib and DMSO scores for H358 Luciferase-dox and NICD3-dox conditions. Dashed line indicates line of equivalence (genes with equal scores in luciferase and NICD3 conditions). Negative scores indicate stronger depletion in sotorasib than DMSO. **B** Western blot of EMT and Rho-regulator Lck after 72 h of sotorasib with or without dox. **C** Western blot of Rock2 and vimentin over a 72 h time course in H358 cells with or without dox.

DISCUSSION

Outside of the developmental context, Notch3 signaling remains largely understudied in contrast to the plethora of papers describing Notch1 and Notch2 transcriptional regulation. Here, we investigate the transcriptional landscape of Notch3 in Kras-mutant lung adenocarcinoma with the eventual goal of discovering and targeting pathways which promote tumor growth and progression.

By integrating RNA-sequencing with Cut&Run data, we are able to identify differentially expressed genes proximal to NICD-V5 peaks, nominating Notch3 direct targets that include Rho GTPase and lung lineage-specific genes. We demonstrate that NICD3 transcriptional activity promotes a epithelial-to-mesenchymal transition, and propose NICD3 as a negative regulator of tumor suppressors. We further identify Notch3 as a modulator of resistance to Kras(G12C) inhibition, likely through EMT pathways as demonstrated by CRISPRi screen. Intriguingly, Slug contained only a weak Notch3 peak in its promoter while Snail had none, suggesting that either NICD3 modulates these genes either through enhancer-dependent regulation or in an indirect manner. The other hit that clustered with the Snail family proteins, Caudal-related family member CDX1, was imputed by VIPER as a co-transcriptional regulator of the Notch signature[40]. Interestingly, the CDX1 transcription factor was first identified as a fetal intestinal marker of hindgut development specifically expressed during the endoderm to epithelial transition[41]. CDX1 was later found as a regulator epithelial-to-mesenchymal transition in epicardial progenitor cells and their differentiation into vascular smooth muscle cells[42], a process which also requires Notch3 signaling[43]. Intriguingly, pericytes, which have been identified as the primary lung cell type expressing Notch3, are believed to be the progenitor cell of origin for coronary artery smooth muscle[44]. More recently, CDX1 loss has been implicated as a driver of

differentiation loss in colorectal cancer, suggesting that its functionality may be context specific[45].

The generalizability of our studies is necessarily limited by the overexpression of NICD3, particularly as Notch signaling is highly dose-sensitive in the context of development. Though such a model may be more relevant in the tumor context where both Notch ligands and receptors area often overexpressed, these studies are primarily intended as hypotheses-generating. Promising findings will require further validation through *in vivo* modeling of tumor-stroma interactions and analysis of patient cohort data.

Future work prioritizing ligand-induced gene expression changes will help narrow the relevant targets, such as the Lck-PAK1/RhoV-PAK1 signaling axes. We find it highly intriguing that Kras inhibition results in marked overexpression of RhoV in NICD-induced cells, particularly given recent reports of high RhoV expression as prognostic of worse survival outcomes and targeted therapy resistance among LUAD patients[46–48] (**Supp. Figure 3.7**). If PAK1 is truly the downstream target of RhoV, as well as the mediator of NICD-dependent Rho activation, it would be fascinating to test whether a PAK1-specific inhibitor could reverse the effects of Notch activation, including Kras(G12C) inhibitor resistance, in LUAD more broadly.

It remains unclear exactly how EMT functions as a resistance mechanism to antagonize covalent Kras inhibition. However, recent data indicates its relevance: A pre- and post-mortem study of a relapsed Kras-G12C mutant LUAD patient, despite finding no additional mutations in Kras itself, found evidence of upregulated AKT, mTOR, and Notch signaling in tumor biopsies after AMG-510 treatment[49]. The authors also discovered robust EMT pathway upregulation in post-treatment tumor intrinsic and extrinsic local tumor microenvironment samples, as well as

downregulation of immune-related gene signatures, confirming the multi-factorial nature of drug resistance and highlighting the need for a combinatorial approach.

Here, we nominate Notch as a potential mediator of resistance and point of therapeutic intervention. While pan-Notch targeting gamma-secretase inhibitors have shown limited response in clinical trials at the expense of non-trivial side effects[50], there is arguably a role for receptor-specific targeting, in conjunction with Kras inhibition, to prevent the evolution of resistant clones. We further hope that by studying the downstream resistance mechanisms engaged by Notch as well as other developmental pathways in solid tumors, it will be possible to discover context-specific transcriptional states required for tumor progression with the ultimate goal of improving our ability to more precisely predict and target cancer evolution, rather than as a mere disease of proliferation.

MATERIALS AND METHODS

Cell culture and Reagents

The human lung cancer cell lines H358, H441, H1437 and H1573 were purchased from ATCC. The H358 dCas9 parental line was a gift from K. Lou and Luke Gilbert (UCSF). The mouse cell line KPY-867 was derived from dissociated lung adenocarcinoma primary cells from the $Kras^{LSLG12D}$ $p53^{fl/fl}$ YFP mouse model. Human cell lines were cultured in RPMI1640 medium (Corning 17-105-CV) and KPY-867 in DMEM (Corning 15-103-CV). Base media was supplemented with 10% bovine growth serum (Hyclone) and 1% penicillin-streptomycin-glutamine (Gibco), and all cell lines were cultured in a humidified CO_2 incubator at 37C. Human cell lines were authenticated by STR profiling and all cell lines were routinely tested for mycoplasma. AMG510 (Kras inhibitor) was obtained from MedChemExpress. Doxycycline (Sigma) was used for induction at 100 ng/ml, and refreshed in culture every 24 h until assay endpoint unless otherwise indicated. Plasmids containing Luciferase-V5 and NICD3-V5 inserts (gift from David Sabatini & Kris Wood, Addgene plasmids #64649 and #64623) were cloned into pLenti CMVtight eGFP Puro and pLenti CMVtight eGFP Neomycin using InFusion (Takara). Stable rtTA expressing cell lines were generated using pLenti CMV rtTA3 Blast. The Tet-On Advanced CMVtight and rtTA3 vectors were a gift from Eric Campeau (Addgene plasmids #26431, #27569 and #26429).

Lentiviral production and cell infection

To produce lentivirus, low-passage HEK293Ts were transfected with delta8.2 and VSVG packaging vectors together with the transfer plasmid using TransIT-293 (Mirus). Viral supernatant was harvested from 72-120 h, pooled, filtered through 0.45 μM filter, aliquoted, and

stored at -80°C until use. Cell lines were infected with viral supernatant and polybrene (8 ug/ml) for 24 h, and selected with the appropriate antibiotic 72 h after infection.

H358 CRISPRi screen

H358 dCas9 parental cells were transformed with rtTA-Blast and Luciferase-V5 or NICD-V5. Guides were designed from the CRISPRi v2 library and cloned into the pLG-21 GFP-puromycin vector. H358 dCas9 Luciferase-V5 and NICD-V5 cells were infected at a MOI of 0.3, selected in puromycin and induced in doxycycline (or mock sterile water for NICD-V5 naive) for 72 h prior to splitting cells for screening at 1000X coverage. Cultures were maintained in DMSO or 0.3 μM of AMG-510 (sotorasib) for 16 days before harvest, with the exception of NICD-Dox DMSO cells which were cultured for 10 days. Genomic DNA was extracted for sgRNA barcode amplification and sequencing. Data analysis was performed using MaGECK MLE package[51] and drug sensitivity scores were calculated by subtraction of the DMSO from the β-sotorasib score.

Antibodies and Western blotting

Cultured cells for protein analysis were directly scraped into ice-cold PBS, resuspended in RIPA lysis buffer (Sigma) supplemented with protease and phosphatase inhibitors (Pierce), and lysed on ice for 30 min. Lysates were clarified at 16,000xg for 10 min, quantified by BCA assay (Pierce), and reduced in 6X Laemelli sample buffer for 20 min at 72°C prior to loading on 10% Tris-Glycine gels. Gels were transferred to PVDF membranes at 100V for 90 min, blocked for 1 h in 5% dry milk in TBST (w/v), and incubated overnight at 4°C with primary antibodies (see supplemental table). The next day, blots were washed three times in TBST and incubated with secondary antibody in milk (Jackson Immunoresearch, 1:5000 for rabbit and 1:2500 for mouse) for 1 h at room temperature before visualization with Clarity Western ECL Substrate (BioRad) or SuperSignal (Pierce). Blots were imaged on the ChemiDoc Imaging system (BioRad).

Immunofluorescence

Luciferase- and NICD3-expressing cell lines were pre-induced for 48 h in doxycycline, plated 25-50,000 cells/cm^2 onto precleaned glass coverslips, and incubated for another 2 days. Cells were fixed in 4% methanol-free paraformaldehyde for 10 min, permeabilized in 0.1% Triton X-100 on ice for 10 min, washed in PBS, and blocked for 1 h in 0.1% Tween-20 with 10% normal goat serum (Jackson Immunoresearch). Coverslips were incubated overnight in primary antibody and then stained with =fluorescently conjugated secondary antibodies for 1 h at room temperature. Coverslips were mounted with ProLong Gold and cured overnight. Cells were imaged on an inverted Lecia microscope with a 100X objective.

RNA isolation, qPCR and library preparation

100-500,000 untreated cells were plated into 6-wells, treated with doxycycline for 48-72 h as indicated, and harvested into TRIzol (Invitrogen). Total RNA was isolated using the Direct-zol RNA kit (Zymo). cDNA was synthesized from 1 ug of purified RNA using the Maxima First Strand cDNA synthesis kit (Thermo Scientific) and qPCR was performed PerfeCta SYBR Green SuperMix (Quanta Biosciences) on a BioRad CFX96 real-time PCR detector. Primers for qPCR are included in Supplemental Table 1.

Cut&Run library preparation and analysis

Cut&Run was performed using the CUT&RUN Assay Kit (Cell Signaling). In brief, H358 and H441 NICD cells were cultured in 100 ng/µl doxycycline for 4 days, dissociated with Accutase (Innovative Cell Technologies), and 100,000 cells used for each reaction. Reactions were incubated overnight at 4C with nutation for the following primary antibodies (Cell Signaling): V5 (#13202), K27Ac (#8173), K4m3 (#9751), rabbit IgG (#6632). 20-40 µl of purified Cut&Run DNA was used as input for standard library preparation (NEBNext Ultra II, E7645). Library

quality was determined using TapeStation analysis (Agilent) before libraries were quantified by Qubit (Invitrogen), pooled, and sequenced. Cut&Run sequencing data was aligned against hg38 and peaks were called using MACS3[52]. Of the ~14,000 V5 peaks identified by MACS2, we used empirically determined thresholds (signal greater than 5 and a score (based on qValue) greater than 100) to filter for 5569 high-confidence peaks.

Proliferation and drug response assays

H358 Luciferase and NICD3 cells, either naive or doxycycline-induced (72 h), were plated into TC-coated (Corning #3596) or ultra-low attachment (Corning #3474) 96-well plates at 2500-5000 cells per well in 200 µl total volume. Cells were treated the next day with drug at the indicated concentrations for 5 days, lysed in 100 µl CellTiterGlo 2.0 (Promega), and luminescence read on a Biotek plate reader.

Subcutaneous xenograft models

In vivo studies were conducted under University of California San Francisco's Institutional Animal Care and Use Committee (IUCAC) approved protocol (Protocol # AN182332-03I) in accordance with approved guidelines. $1x10^6$ naive H441, H358, and H1573 Luciferase and NICD3 cell lines were injected in the flanks of 2-6 month old NSG mice and monitored for growth. Once palpable tumors formed, mice were either maintained on normal chow or administered doxycycline-containing chow (200 mg/kg, Invivogen) which was changed weekly. Tumors were measured 2-3 times weekly until endpoint at which point the mice were sacrificed and tumors preserved in formalin for subsequent studies.

Statistical methods

In vitro experiments were performed in biological triplicate, except for the RNA-sequencing experiment which was performed with four replicates and the Cut&Run, which was performed

with duplicate replicates. The unpaired two-tailed Student *t* test was used to compute statistically significant differences and $P < 0.05$ was considered a cutoff for statistical significance.

REFERENCES

1. Prager, B. C., Xie, Q., Bao, S. & Rich, J. N. Cancer Stem Cells: The Architects of the Tumor Ecosystem. *Cell Stem Cell* **24**, 41–53 (2019).

2. Odoux, C. *et al*. A Stochastic Model for Cancer Stem Cell Origin in Metastatic Colon Cancer. *Cancer Research* **68**, 6932–6941 (2008).

3. Driessens, G., Beck, B., Caauwe, A., Simons, B. D. & Blanpain, C. Defining the mode of tumour growth by clonal analysis. *Nature Publishing Group* **488**, 527–530 (2012).

4. Chen, J. *et al*. A restricted cell population propagates glioblastoma growth after chemotherapy. *Nature* **488**, 522–526 (2012).

5. Ricci-Vitiani, L. *et al*. Identification and expansion of human colon-cancer-initiating cells. *Nature* **445**, 111–115 (2007).

6. Zhang, S. *et al*. Identification and Characterization of Ovarian Cancer-Initiating Cells from Primary Human Tumors. *Cancer Research* **68**, 4311–4320 (2008).

7. Batlle, E. & Clevers, H. Cancer stem cells revisited. *Nature Medicine* **23**, 1124–1134 (2017).

8. De Sousa E Melo, F. *et al*. A distinct role for Lgr5+ stem cells in primary and metastatic colon cancer. *Nature* **543**, 676–680 (2017).

9. Shimokawa, M. *et al*. Visualization and targeting of LGR5+ human colon cancer stem cells. *Nature* **545**, 187–192 (2017).

10. Laughney, A. M. *et al*. Regenerative lineages and immune-mediated pruning in lung cancer metastasis. *Nat Med* **26**, 259–269 (2020).

11. Figarol, S. *et al*. *Farnesyltransferase inhibition overcomes the adaptive resistance to osimertinib in* EGFR *-mutant NSCLC*. http://biorxiv.org/lookup/doi/10.1101/2022.04.01.486707 (2022) doi:10.1101/2022.04.01.486707.

12. Campeau, E. *et al*. A Versatile Viral System for Expression and Depletion of Proteins in Mammalian Cells. *PLoS ONE* **4**, e6529 (2009).

13. Borggrefe, T. & Oswald, F. The Notch signaling pathway: Transcriptional regulation at Notch target genes. *Cell. Mol. Life Sci.* **66**, 1631–1646 (2009).

14. Martz, C. A. *et al*. Systematic identification of signaling pathways with potential to confer anticancer drug resistance. *Sci Signal* **7**, ra121–ra121 (2014).

15. Hänzelmann, S., Castelo, R. & Guinney, J. GSVA: gene set variation analysis for microarray and RNA-Seq data. *BMC Bioinformatics* **14**, 7 (2013).

16. Tata, P. R. *et al*. Dedifferentiation of committed epithelial cells into stem cells in vivo. *Nature* **503**, 218–223 (2013).

17. Schwitalla, S. *et al*. Intestinal Tumorigenesis Initiated by Dedifferentiation and Acquisition of Stem-Cell-like Properties. *Cell* **152**, 25–38 (2013).

18. Travaglini, K. J. *et al*. A molecular cell atlas of the human lung from single-cell RNA sequencing. *Nature* **587**, 619–625 (2020).

19. Wang, Y. *et al*. Comprehensive Molecular Characterization of the Hippo Signaling Pathway in Cancer. *Cell Reports* **25**, 1304-1317.e5 (2018).

20. Yu, G., Wang, L.-G. & He, Q.-Y. ChIPseeker: an R/Bioconductor package for ChIP peak annotation, comparison and visualization. *Bioinformatics* **31**, 2382–2383 (2015).

21. Skene, P. J. & Henikoff, S. An efficient targeted nuclease strategy for high-resolution mapping of DNA binding sites. *Elife* **6**, 576 (2017).

22. Skene, P. J., Henikoff, J. G. & Henikoff, S. Targeted in situ genome-wide profiling with high efficiency for low cell numbers. *Nat Protoc* **13**, 1006–1019 (2018).

23. Zhu, Q., Liu, N., Orkin, S. H. & Yuan, G.-C. CUT&RUNTools: a flexible pipeline for CUT&RUN processing and footprint analysis. *Genome Biol* **20**, 192 (2019).

24. Bailey, T. L., Johnson, J., Grant, C. E. & Noble, W. S. The MEME Suite. *Nucleic Acids Res* **43**, W39–W49 (2015).

25. Yashiro-Ohtani, Y. *et al*. Long-range enhancer activity determines Myc sensitivity to Notch inhibitors in T cell leukemia. *Proc Natl Acad Sci USA* **111**, E4946–E4953 (2014).

26. Andersson, R. & Sandelin, A. Determinants of enhancer and promoter activities of regulatory elements. *Nat Rev Genet* **21**, 71–87 (2020).

27. Balbin, O. A. *et al*. Reconstructing targetable pathways in lung cancer by integrating diverse omics data. *Nat Commun* **4**, 2617 (2013).

28. Su, J. *et al*. TGF-β orchestrates fibrogenic and developmental EMTs via the RAS effector RREB1. *Nature* 1–28 (2020) doi:10.1038/s41586-019-1897-5.

29. Ohkubo, T. & Ozawa, M. The transcription factor Snail downregulates the tight junction components independently of E-cadherin downregulation. *Journal of Cell Science* **117**, 1675–1685 (2004).

30. Moore, A. R., Rosenberg, S. C., McCormick, F. & Malek, S. RAS-targeted therapies: is the undruggable drugged? *Nat Rev Drug Discov* **19**, 533–552 (2020).

31. Hong, D. S. *et al*. KRAS ^{G12C} Inhibition with Sotorasib in Advanced Solid Tumors. *N Engl J Med* **383**, 1207–1217 (2020).

32. Skoulidis, F. *et al*. Sotorasib for Lung Cancers with *KRAS* p.G12C Mutation. *N Engl J Med* **384**, 2371–2381 (2021).

33. Awad, M. M. *et al*. Acquired Resistance to KRAS ^{G12C} Inhibition in Cancer. *N Engl J Med* **384**, 2382–2393 (2021).

34. Sequist, L. V. *et al*. Genotypic and histological evolution of lung cancers acquiring resistance to EGFR inhibitors. *Sci Transl Med* **3**, 75ra26-75ra26 (2011).

35. Adachi, Y. *et al*. Epithelial-to-Mesenchymal Transition is a Cause of Both Intrinsic and Acquired Resistance to KRAS G12C Inhibitor in KRAS G12C–Mutant Non–Small Cell Lung Cancer. *Clin Cancer Res* **26**, 5962–5973 (2020).

36. Solanki, H. S. *et al*. Cell Type–specific Adaptive Signaling Responses to KRAS ^{G12C} Inhibition. *Clin Cancer Res* 1078-0432.CCR-20–3872 (2021) doi:10.1158/1078-0432.CCR-20-3872.

37. Xue, J. Y. *et al*. Rapid non-uniform adaptation to conformation-specific KRAS(G12C) inhibition. *Nature* 1–23 (2020) doi:10.1038/s41586-019-1884-x.

38. Xu, Y., Huang, S., Liu, Z.-G. & Han, J. Poly(ADP-ribose) Polymerase-1 Signaling to Mitochondria in Necrotic Cell Death Requires RIP1/TRAF2-mediated JNK1 Activation. *Journal of Biological Chemistry* **281**, 8788–8795 (2006).

39. Tseng, P.-C. *et al*. Epithelial-to-mesenchymal transition hinders interferon-γ-dependent immunosurveillance in lung cancer cells. *Cancer Letters* **539**, 215712 (2022).

40. Alvarez, M. J. *et al*. Functional characterization of somatic mutations in cancer using network-based inference of protein activity. *Nat Genet* **48**, 838–847 (2016).

41. Silberg, D. G., Swain, G. P., Suh, E. R. & Traber, P. G. Cdx1 and cdx2 expression during intestinal development. *Gastroenterology* **119**, 961–971 (2000).

42. Chu, M. *et al*. A novel role of CDX1 in embryonic epicardial development. *PLoS One* **9**, e103271 (2014).

43. Tefft, J. B. *et al*. Notch1 and Notch3 coordinate for pericyte-induced stabilization of vasculature. *Am J Physiol Cell Physiol* **322**, C185–C196 (2022).

44. Volz, K. S. *et al*. Pericytes are progenitors for coronary artery smooth muscle. *Elife* **4**, e10036 (2015).

45. Luk, I. Y. *et al*. Epithelial de-differentiation triggered by co-ordinate epigenetic inactivation of the EHF and CDX1 transcription factors drives colorectal cancer progression. *Cell Death Differ* (2022) doi:10.1038/s41418-022-01016-w.

46. Shepelev, M. V. & Korobko, I. V. The RHOV gene is overexpressed in human non–small cell lung cancer. *Cancer Genetics* **206**, 393–397 (2013).

47. Chen, H. *et al*. Overexpression of RhoV Promotes the Progression and EGFR-TKI Resistance of Lung Adenocarcinoma. *Front. Oncol.* **11**, 619013 (2021).

48. Zhang, D. *et al*. RHOV promotes lung adenocarcinoma cell growth and metastasis through JNK/c-Jun pathway. *Int. J. Biol. Sci.* **17**, 2622–2632 (2021).

49. Tsai, Y. S. *et al*. Rapid idiosyncratic mechanisms of clinical resistance to KRAS G12C inhibition. *Journal of Clinical Investigation* **132**, e155523 (2022).

50. McCaw, T. R. *et al*. Gamma Secretase Inhibitors in Cancer: A Current Perspective on Clinical Performance. *The Oncologist* **26**, e608–e621 (2021).

51. Li, W. *et al*. Quality control, modeling, and visualization of CRISPR screens with MAGeCK-VISPR. *Genome Biol* **16**, 281 (2015).

52. Zhang, Y. *et al*. Model-based analysis of ChIP-Seq (MACS). *Genome Biology* **9**, R137 (2008).

CHAPTER 4

CONCLUSIONS

SUMMARY OF FINDINGS

The complex nature of Notch signaling defies an easy or straightforward understanding, yet, from the first identification of mutant *Drosophila* wings to the ever-expanding list of cancers co-opting pathogenic Notch signaling[1], it remains a subject of great interest due to its intricate and fundamental involvement in both development and oncogenesis. We explore Notch signaling in the lung adenocarcinoma context, utilizing both pan-Notch gamma-secretase inhibitors and expression of V5-tagged NICD3 to determine the consequences of endogenous activation and chromatin binding.

In Chapter 2, we describe the generation of primary cell lines from the $Kras^{LSL\text{-}G12D}$ $p53^{fl/fl}$ genetically engineered mouse model and find that both the original primary cells as well as the derived mouse cell lines exhibit limited dependency on Notch signaling activity. We also examine human LUAD cell lines harboring no identified Notch mutations to show that while gamma-secretase inhibitors are functional in these cell lines, we find no evidence of dependency in the context of 2D or 3D growth in *vitro*.

We therefore turn to the generation of inducible NICD3 models in Chapter 3 and study the transcriptomic and epigenomic activity of Notch3 in Kras-mutant lung adenocarcinoma cell lines. We observe the adoption of a mesenchymal-like state in our Kras-mutant mouse and human lines, and find that pathway analysis enriches for migration-related pathways, as well as downregulation of focal adhesion components in the human cell lines. We focus upon the human cell lines and identify a number of common NICD3-induced pathways, including upregulation of mTORC and downregulation of growth-factor related pathways. We show broad dysregulation of lung lineage-specific genes in response to NICD3 expression, including Hippo/YAP target genes and AT1/mucous lineage markers, the cumulative effect of which is to promote a less-

differentiated phenotype relative to the parental cell lines. We further link NICD3 signaling to the adoption of mesenchymal features in support of the de-differentiation phenotype, resulting in re-clustering of epithelial cell lines with mesenchymal ones and a highly reproducible increase in tumor growth. We also use Cut&Run from the H358 NICD3-V5 cell line to show that these transcriptional changes occur in both a direct and indirect manner, and discover a novel role for Notch3 in direct transcriptional regulation of Rho pathway-related genes.

Finally, we use our inducible H358 KrasG12C-mutant cell line to investigate a potential role for Notch3 signaling as a resistance mechanism to Kras(G12C) inhibition. We demonstrate that NICD3 expression is sufficient to inhibit the anti-proliferative effects of G12C inhibitors on cell viability, cell cycle arrest and apoptosis. We find that NICD3 expression delays G12i-mediated repression of the PI3K/AKT but not the MAPK signaling axis, suggesting a potential targetable avenue of resistance, as well as upregulating proliferative signatures in the expression data. Finally, we performed a focused CRISPRi screen in the setting of NICD-induced G12C inhibitor resistance which revealed known transcriptional regulators of EMT, including Snail, Slug and CDX1. Together, this data reinforces the biological and therapeutic relevance of EMT cell state to LUAD and elucidates the role of Notch as potential modulator of this mechanism.

DISCUSSION AND FUTURE DIRECTIONS

Notch3 in tumorigenesis: therapeutic opportunities and cell type-specific functions

With its multi-factorial layers of regulation and cell context specific effects, the Notch developmental pathway is at once both an attractive and daunting therapeutic target. However, the highly specific and non-essential (relative to Notch1/2) function of Notch3 in adult cellular development provides a so-called "window" for disease-specific cytotoxicity. In addition, the

role of Notch3 in lung progenitor cells in maintenance of stemness and self-renewal, as well as evidence of Notch-dependent transdifferentiation in the adult murine lung[2], strongly suggest that the LUAD progenitor state is likely to either express, or be poised to express, Notch3 in a non-redundant manner. Importantly, it is likely that stemness is not maintained by a single cell population but rather an environmental niche supported by ligand-expressing ("sender") cells neighboring to the "receiver" receptor cell that activate their own signaling program - or that stemness might even be modulated in cells expressing both receptor and ligand, capable of inducing their own cross-talk. Though outside of the scope of this particular work, it has been shown that Notch3 upregulation is associated with the immature thymocyte state, leading to the hypothesis that it regulates the pre-T cell receptor checkpoint[3]. In contrast, Notch1 is involved in initial T cell lineage commitment of bone-marrow derived lymphoid progenitors[4] and in intrathymic T cell fate[5], suggesting that the structural and developmental expression differences in Notch receptors evolved to allow fate-specific regulation through a shared signaling mechanism. Unsurprisingly, high Notch3 expression, possibly through protein stabilization via PEST domain mutation, is observed in T-cell acute lymphoblastic leukemia[6] and Notch3 has been shown to have a role in disease pathogenesis[7]. Notch3 overexpression has also demonstrated in aggressive ovarian carcinomas[8]. ChIP-chip data from ovarian cancer cell line models described Notch3 transcriptional regulation of the mitotic spindle regulator DLGAP5[9], which was not upregulated in our datasets suggesting cell-context specific regulation. Notch3 interactome data using protein microarrays also discovered the E3 ubiquitin ligase WWP2 as a novel and NICD3-specific negative regulator and overexpression of WWP2 decreased tumor development[10], indicating a potential avenue of specifically targeting activated Notch3 downstream of receptor expression. Together, these data support a role for Notch transcriptional

regulation in tumorigenesis contexts outside of lung cancer and broaden the generalizability of Notch3 targeting in oncogenesis.

Epigenetic regulation of cell state and tumor progression in Kras-mutant LUAD

Our findings underscore the contribution of Notch3 transcriptional activity to promote an epithelial-to-mesenchymal transitional cell state and implicate this state in resistance to targeted Kras therapies. Given that our initial studies were motivated by identification of a Notch-high cell population in the primary KP LUAD GEMM, we will briefly discuss parallel findings in single cell ATAC-seq and RNA-seq data from development timepoints through tumor progression in this model as described in two concomitant studies published through a multi-group collaborative effort by the Buenrostro, Tammela and Jacks labs using the SPC-Cre KP-tdTomato (KPT) LUAD model[11,12] with the goal of providing additional context for this work.

In LaFave et al., the authors use single-cell chromatin accessibility (ATAC-seq) over early and late timepoints in tumorigenesis to define master transcription factor programs shared by distinct cell states[11]. They establish CEBPA and TEAD/GATA as AT2- and AT1-specific regulators, respectively, and find that the ATAC-seq landscape of early tumor cells closely correlates with an AT2-type program but that this is gradually lost through progression into the mature adenocarcinoma state. The authors are able to model this progression through a RNA-Velocity-like analysis of differential ATAC peaks and define a set of transcriptional "modules" that KP cells transit through during progression. Importantly for our purposes, the authors show a distinct EMT-related module that marks a transition point between the early and late stages of tumor progression, and demonstrate that this module is defined by progressive adoption of TGF-β, secretory, and extracellular matrix gene programs. This is strongly reminiscent of the NICD3-

induced cell state we observe in our mouse and human Kras-mutant cell lines, which all revealed upregulation of cytokine/secretory pathways in addition to downregulation of adhesion and cytoskeletal programs. We also found striking *downregulation* of lung-lineage specifying genes by NICD3, as well as evidence of increased tumor growth capacity *in vivo*, which may correspond to their description of expansive lineage fidelity loss in cell states during tumor progression.

In parallel, Marjanovic et al. examined the heterogeneity of single-cell expression using the same KPT LUAD model through early adenoma to late adenocarcinoma states. Importantly, they found that even in the absence of other somatic alterations, this model demonstrated increasing phenotypic diversity over tumor progression and, reminiscent of LaFave et al.'s work, that tumor cells undergo loss of AT2 lineage-specific expression and gain transcription programs identified with primordial endodermal (specifically gut) developmental regulators. In late adenocarcinoma, they identified a subpopulation with expressing mouse embryonic fibroblast markers consistent with EMT which they claimed was exclusive to this late stage, which they argued was evidence that LUAD tumors retain their epithelial identity for most of their *in situ* tumor development. In defining transcriptional programs along the tumor evolutionary continuum, the authors also found a "mixed AT1/AT2" early population that partially expressed the "late-stage" EMT program, which they then termed as a high-plasticity cell state. Their functional studies implicated this high-plasticity state as cells with high differentiation potential but relatively low proliferation, enabling them to escape a transient pulse of cisplatin treatment. The authors also annotated specific markers for AT2-like, embryonic liver-like, and mixed-program cell states, corresponding to gradual disease progression. They further established that individual cells could co-express these markers, which they interpreted as evidence of

transitional cell states. Intriguingly, these markers were lysozyme (AT2), claudin-2 (embryonic liver), and claudin-4 (mixed). The involvement of claudin in marking the latter two, more advanced cell types suggest that the tight junction may be particularly relevant to identifying cell state for reasons yet unknown. We identified a *downregulation* of claudin-1 among other family members by NICD3 at the transcriptional and protein level in the human LUAD cell lines but no change in claudin-4, while claudin-2 was slightly upregulated by NICD3 in the KPY mouse cell line (data not shown), and indeed the strongly downregulated focal adhesion highlighted by GSVA signatures often included the claudin family genes. No claudin family genes were directly marked by a Notch promoter, indicating that NICD3 likely regulates these genes in an indirect manner through upregulation of repressive factors. Notably, we find that NICD3 strongly upregulates EMT-regulators Snail and Slug and both of these transcription factors have been shown to act as repressors of claudin-1 in epithelial cells[13]. While we would not necessarily expect NICD3-regulated gene expression to strictly overlap with the findings from the KPT GEMM, it is intriguing that Notch3 can regulate a similar set of gene pathways and that Snail, Slug, and CDX1 (a primitive endodermal/hindgut transcriptional regulator) are required for NICD3-induced resistance to targeted therapy.

Our transcriptomic and epigenomic survey of NICD3 in LUAD cell lines is largely preliminary, and further characterization may greatly increase the potential impact of this work. First, the epigenetic mechanisms of Notch-mediated regulation of the master EMT regulators Snail, Slug and CDX1 remain unknown. We propose that this may occur through FOXO1 inactivation, since both Snail and Slug are well-known to be repressed by FOXO1 and we also observe marked downregulation of the FOXO1-target p21 in NICD3-expressing cells; however, we find in preliminary work that FOXO1 abundance counterintuitively increases with NICD3

expression (data not shown). It is well known, however, that AKT-dependent phosphorylation destabilizes FOXO1 and promotes its nuclear export, and we have observed that NICD3 upregulates AKT/mTORC-related signatures, so we believe there may be compensatory upregulation or stabilization mechanisms that stabilize FOXO1 expression in an inhibited state, though this is purely speculative. Second, EMT historically has been used as a marker of "invasive potential" and *in vitro* phenotypes of migration, but it is poorly understood how precisely EMT contributes to tumor progression and chemoresistance. Our NICD3 model represents an opportunity to further explore the consequences and mechanisms of these EMT-induced phenotypes, which we argue are distinct from cellular morphology as we observe re-gaining of the epithelial appearance with Kras inhibition of NICD3-expressing cells (data not shown), despite a lack of regained tight junction proteins, N-cadherin downregulation, or E-cadherin upregulation (**Figure 3.16 B**). Indeed, Kras inhibition in control H358 cell lines demonstrate marked downregulation of Rho family member Lck, Snail, and N-cadherin alongside upregulation of ZO-3, suggesting that Kras inhibition itself can impact the expression of EMT-related proteins. Together, these suggest that further work relying on the cellular morphology or vimentin as a readout of EMT may miss the *transcriptional* contribution of EMT regulators in absence of a TGF-β-like effect, and that while morphologic and tumor growth/chemoresistance phenotypes may co-occur, these are in fact separable from one another and should be studied individually.

Conclusions

The work presented herein suggest a rationale for the study of Notch-driven transcriptional programs in LUAD and generate integrative transcriptomic and epigenomic datasets to facilitate the study of direct versus indirect Notch regulation. Our data reveal the potential of Notch3 as a

regulator of EMT not only with respect to cellular morphology, but also in the setting of resistance to novel Kras inhibitors. Further studies are required to elucidate the role of Notch signaling in LUAD patients with intrinsic or acquired resistance to Kras inhibitors and identify potential therapeutic interventions as such inhibitors are more widely adopted in clinical settings.

REFERENCES

1. Aster, J. C., Pear, W. S. & Blacklow, S. C. The Varied Roles of Notch in Cancer. *Annu. Rev. Pathol. Mech. Dis.* **12**, 245–275 (2017).

2. Siebel, C. & Lendahl, U. Notch Signaling in Development, Tissue Homeostasis, and Disease. *Physiological Reviews* **97**, 1235–1294 (2017).

3. Felli, M. P. *et al*. Expression pattern of notch1, 2 and 3 and Jagged1 and 2 in lymphoid and stromal thymus components: distinct ligand-receptor interactions in intrathymic T cell development. *Int Immunol* **11**, 1017–1025 (1999).

4. Radtke, F. *et al*. Deficient T cell fate specification in mice with an induced inactivation of Notch1. *Immunity* **10**, 547–558 (1999).

5. Fowlkes, B. J. & Robey, E. A. A reassessment of the effect of activated Notch1 on CD4 and CD8 T cell development. *J Immunol* **169**, 1817–1821 (2002).

6. Bernasconi-Elias, P. *et al*. Characterization of activating mutations of NOTCH3 in T-cell acute lymphoblastic leukemia and anti-leukemic activity of NOTCH3 inhibitory antibodies. **35**, 6077–6086 (2016).

7. Ferrandino, F. *et al*. Intrathymic Notch3 and CXCR4 combinatorial interplay facilitates T-cell leukemia propagation. *Oncogene* **37**, 6285–6298 (2018).

8. Park, J. T. *et al*. Notch3 gene amplification in ovarian cancer. *Cancer Res* **66**, 6312–6318 (2006).

9. Chen, X. *et al*. Defining NOTCH3 Target Genes in Ovarian Cancer. *Cancer Res* **72**, 2294–2303 (2012).

10. Jung, J.-G. *et al*. Notch3 Interactome Analysis Identified WWP2 as a Negative Regulator of Notch3 Signaling in Ovarian Cancer. *PLoS Genet* **10**, e1004751-16 (2014).

11. LaFave, L. M. *et al*. Epigenomic State Transitions Characterize Tumor Progression in Mouse Lung Adenocarcinoma. *Cancer Cell* **38**, 212-228.e13 (2020).

12. Marjanovic, N. D. *et al*. Emergence of a High-Plasticity Cell State during Lung Cancer Evolution. *Cancer Cell* **38**, 229-246.e13 (2020).

13. Martínez-Estrada, O. M. *et al*. The transcription factors Slug and Snail act as repressors of Claudin-1 expression in epithelial cells. *Biochem J* **394**, 449–457 (2006).

Publishing Agreement

It is the policy of the University to encourage open access and broad distribution of all theses, dissertations, and manuscripts. The Graduate Division will facilitate the distribution of UCSF theses, dissertations, and manuscripts to the UCSF Library for open access and distribution. UCSF will make such theses, dissertations, and manuscripts accessible to the public and will take reasonable steps to preserve these works in perpetuity.

I hereby grant the non-exclusive, perpetual right to The Regents of the University of California to reproduce, publicly display, distribute, preserve, and publish copies of my thesis, dissertation, or manuscript in any form or media, now existing or later derived, including access online for teaching, research, and public service purposes.

DocuSigned by:
Elizabeth Hwang
FD18CB4DA584464...
Author Signature

8/23/2022
Date